Fiber Grating Sensors

Alan D. Kersey, Michael A. Davis, Heather J. Patrick, Michel LeBlanc, K. P. Koo, *Member, IEEE*, C. G. Askins, M. A. Putnam, and E. Joseph Friebele

(Invited Paper)

***Abstract*— We review the recent developments in the area of optical fiber grating sensors, including quasi-distributed strain sensing using Bragg gratings, systems based on chirped gratings, intragrating sensing concepts, long period-based grating sensors, fiber grating laser-based systems, and interferometric sensor systems based on grating reflectors.**

I. Introduction

THE advantages of optical fiber sensing are well known and have been widely extolled in the research literature on the subject. Fiber sensors have, however, resulted in relatively few real commercial successes, and the technology remains in many instances, laboratory-based at the prototype stage. The reason for this is becoming clear to most researchers in the field: many fiber optic sensors were developed to displace conventional electro-mechanical sensor systems, which are well established, have proven reliability records and manufacturing costs. Thus, even though fiber sensors offer important advantages such as electrically passive operation, EMI immunity, high sensitivity, and multiplexing capabilities, market penetration of this technology has been slow to develop. In applications where fiber sensors offer new capabilities, however, such as distributed sensing, fiber sensors appear to have a distinct edge over the competition. Fiber Bragg gratings (FBG's) and other grating-based devices are examples of the type of sensors which provide this capability.

Gratings are simple, intrinsic sensing elements which can be photo-inscribed into a silica fiber [1]–[6] and have all the advantages normally attributed to fiber sensors. In addition, the devices have an inherent self referencing capability and are easily multiplexed in a serial fashion along a single fiber [7]–[9]. Grating-based sensors appear to be useful for a variety of applications. In particular the area of distributed embedded sensing in materials for creating "smart structures" is of primary interest. Here fibers with sensor arrays can be embedded into the materials to allow measurement of parameters such as load, strain, temperature, and vibration, from which the health of the structure can be assessed and tracked on a real-time basis. Gratings may also prove to be useful as the optical sensing element in a range of other fiber sensor configurations; grating-based chemical sensors, pressure sensors, and accelerometers are examples.

Manuscript received May 5, 1997. This work was supported by the Office of Naval Research (ONR), Defense Advanced Research Projects Agency (DARPA), and the Federal Highway Administration (FHWA).

The authors are with the Optical Sciences Division, Naval Research Laboratory, Washington, DC 20375 USA.

Publisher Item Identifier S 0733-8724(97)05919-7.

This paper will review developments in the area of grating based sensors, including basic quasi-distributed sensors based on Bragg gratings, chirped grating sensing, fiber Bragg grating laser sensors, long-period grating sensors and interferometric configurations based on gratings. The techniques discussed will primarily focus on the measurement of strain, but systems have also been used for temperature measurements.

II. Bragg Grating Point Sensors

The basic principle of operation commonly used in a FBG-based sensor system is to monitor the shift in wavelength of the returned "Bragg" signal with the changes in the measurand (e.g., strain, temperature). The Bragg wavelength, or resonance condition of a grating, is given by the expression [7]

$$\lambda_B = 2n\Lambda \tag{1}$$

where Λ is the grating pitch and n is the effective index of the core. With such a device, injecting spectrally broadband source of light into the fiber, a narrowband spectral component at the Bragg wavelength is reflected by the grating. In the transmitted light, this spectral component is missing, as depicted in Fig. 1. The bandwidth of the reflected signal depends on several parameters, particularly the grating length, but typically is $\sim$0.05 to 0.3 nm in most sensor applications. Perturbation of the grating results in a shift in the Bragg wavelength of the device which can be detected in either the reflected or transmitted spectrum, as shown.

Most of the work on fiber Bragg grating sensors has focused on the use of these devices for providing quasi-distributed point sensing of strain or temperature. The strain response arises due to both the physical elongation of the sensor (and corresponding fractional change in grating pitch), and the change in fiber index due to photoelastic effects, whereas the thermal response arises due to the inherent thermal expansion of the fiber material and the temperature dependence of the refractive index. The shift in Bragg wavelength with strain and temperature can be expressed using

$$\Delta\lambda_B = 2n\Lambda\left(\left\{1-\left(\frac{n^2}{2}\right)[P_{12}-\nu(P_{11}+P_{12})]\right\}\varepsilon + \left[\alpha+\frac{\left(\frac{dn}{dT}\right)}{n}\right]\Delta T\right) \tag{2}$$

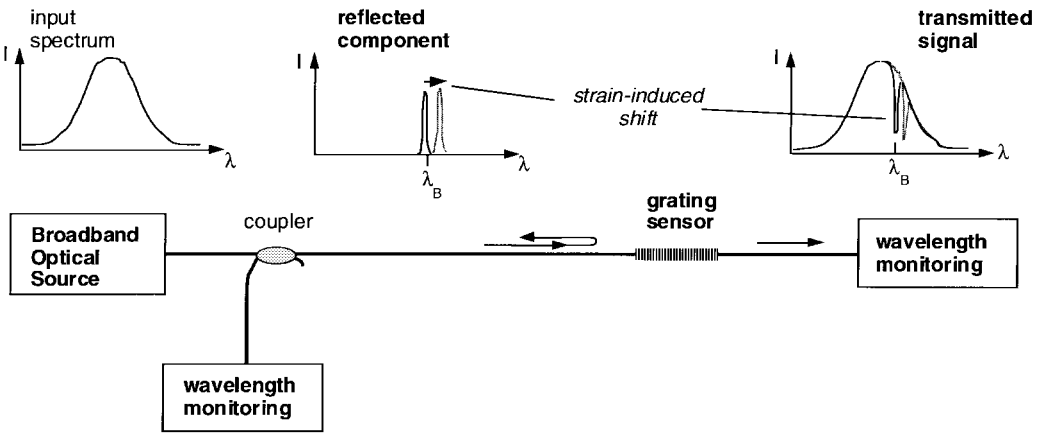

Fig. 1. Basic Bragg grating-based sensor system with transmissive or reflective detection options.

where ε is the applied strain, $P_{i,j}$ coefficients are the Pockel's (piezo) coefficients of the stress-optic tensor, ν is Poisson's ratio, and α is the coefficient of thermal expansion (CTE) of the fiber material (e.g., silica), and ΔT is the temperature change. The factor $\{(n^2/2)[P_{12} - \nu(P_{11} + P_{12})]\}$ has a numerical value of $\approx$0.22. The measured strain response at constant temperature is found to be

$$\frac{1}{\lambda_B}\frac{\delta\lambda_B}{\delta\varepsilon} = 0.78 \times 10^{-6}\,\mu\varepsilon^{-1}. \tag{3}$$

This responsivity gives a "rule-of-thumb" measure of the grating shift with strain of 1 nm per 1000 $\mu\varepsilon$ at 1.3 μm. In silica fibers, the thermal response is dominated by the dn/dT effect, which accounts for $\sim$95% of the observed shift. The normalized thermal responsivity at constant strain is

$$\frac{1}{\lambda_B}\frac{\delta\lambda_B}{\delta T} = 6.67 \times 10^{-6}\,^{\circ}\mathrm{C}^{-1}. \tag{4}$$

A wavelength resolution of $\sim$1 pm (0.001 nm) is required (at $\lambda_B \sim 1.3$ μm) to resolve a temperature change of $\sim$0.1 °C, or a strain change of 1 μstrain. Although this wavelength resolution is attainable using laboratory instrumentation such as spectrum analyzers and tunable lasers, the ability to resolve changes on this order using small, packaged electro-optics units is a challenge, and this has been the focus of a considerable amount of research work in the grating sensor field.

The nature of the output of Bragg gratings provide these sensors with a built-in self-referencing capability. As the sensed information is encoded directly into wavelength, which is an absolute parameter, the output does not depend directly on the total light levels, losses in the connecting fibers and couplers, or source power. This is widely acknowledged as one of the most important advantages of these sensors. The wavelength encoded nature of the output, however, also facilitates wavelength division multiplexing by allowing each sensor to be assigned to a different "slice" of the available source spectrum. This enables quasi-distributed sensing of strain, temperature, or potentially other measurands by associating each spectral slice with a particular spatial location. The concept is illustrated in Fig. 2: The upper limit to the number of gratings which can be addressed in this way is a function of the source profile width and the operational wavelength

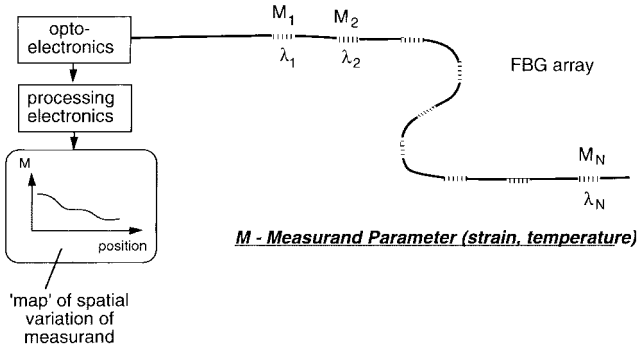

Fig. 2. Quasi-distributed sensor system using FBG elements.

bandwidth required for each grating element. With current gratings it is possible to multiplex 20 or more devices along a single fiber path if the peak strains experienced by the gratings do not exceed $\pm$0.1% ($\pm$1000 μstrain).

Although a wide variety of techniques have been demonstrated for monitoring Bragg wavelength shifts, only certain techniques appear to have the potential for being reduced to a practical, cost-effective instrumentation systems for use in "real-world" applications. Here we review the progress made in the development of such instrumentation systems for static and dynamic strain applications.

The most frequently utilized method for the interrogation of FBG sensors is based on passive broadband illumination of the device: Light with a broad spectrum which covers that of the FBG sensors is input to the system; either the narrowband component reflected by the FBG is directed to a wavelength detection system, or the spectral "notches" in the transmitted are analyzed.

A. Quasi-Static Strain Monitoring

Several techniques have been demonstrated to be quite reliable for performing this wavelength analysis. A ratiometric approach based on the use of broadband filters was the first approach to be demonstrated [10]. This method allows the shift in the FBG wavelength of the sensor element to be assessed by comparing the transmittance of the FBG-reflected light through a filter to that passed through a direct reference

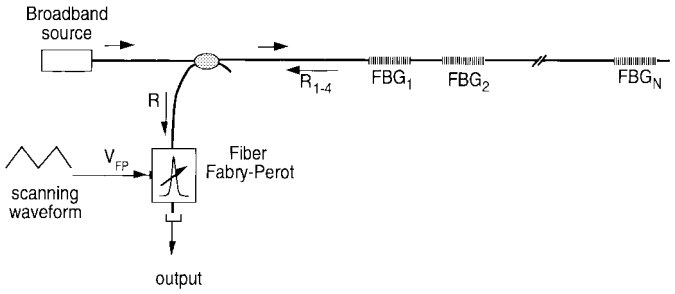

Fig. 3. Scanning filter FBG grating detection technique.

path. Edge or bandpass filters provide a suitable wavelength-dependent loss for this type of detection system. A relatively limited sensitivity is obtained using this approach due to associated problems with the use of bulk-optic filter/collimation components and associated alignment stability. One means to improve on this is to use a fiber device with a wavelength dependent transfer function, such as for example, a fiber wavelength-division multiplexing (WDM) coupler [11], [12]. A resolution $\sim \pm 5$ μstrain, corresponding to $\sim \pm 0.5$ °C has been demonstrated using this approach. Other types of filters, such as biconical fiber filters have been used for this purpose [13].

One of the most successful techniques for interrogating FBG sensors is based on the use of a tunable passband filter for tracking the FBG signal. The most commonly used technique is based on the use of Fabry–Perot (FP) filters [15]–[17], however, acousto-optic filters [18], [19], and FBG-based filters [20], [21] are examples of the types of filter suitable for this. A system based on a scanning FP filter is depicted in Fig. 3. Here, light reflected from an array of Bragg grating sensors is passed through a FP filter which passes one narrowband wavelength component, depending on the spacing between the mirrors in the device. Electrical control of this mirror spacing via piezoelectric stacks allows for tuning the passband wavelength. As the filter is tuned, the passband scans over the return signals from the gratings, and the wavelengths can be determined and recorded from the voltage applied to the filter as the return signals are detected.

In operation, the light reflected from the grating sensors is returned via the coupler to the scanning Fabry–Perot optical filter and to a detector. Typical characteristics of the type of FP used are a free spectral range (FSR) of 50 nm and a bandwidth of $\sim$0.3 nm. This allows as many as 16 individual sensor gratings spaced by $\approx$3 nm to be used. For a FSR of 50 nm, generation of the scanning voltage for the FP filter via a 16-bit digital-to-analog converter produces a minimum resolvable (least significant bit) wavelength shift of approximately 0.8 pm, or an equivalent strain resolution of 0.8 μstrain. Currently available FP filters can be scanned at rates $>$300 Hz, although scan rates to $\sim$1 kHz should be possible.

Fig. 4 shows a comparison of the strain monitored with a scanning-filter demodulated FBG and resistive foil strain gauge when both were strained to $\sim$2000 μstrain. Resolutions on the order of $\sim \pm 1$ μstrain have been achieved with the FP approach, and up to 16 gratings have been multiplexed on a single fiber. The use of an optical switch allows such an

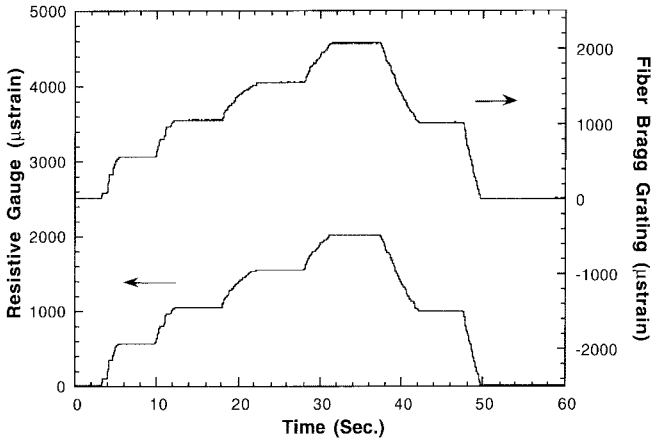

Fig. 4. Comparison between a resistive strain gauge (RSG) and an FGB sensor.

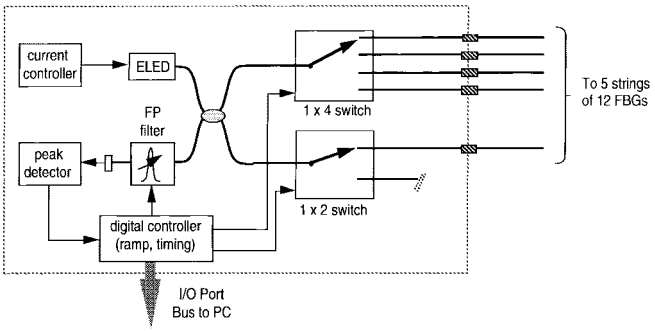

Fig. 5. Schematic diagram of the 60 channel FBG sensor electro-optics system.

instrumentation system to address several "arrays" of gratings, and a system for tracking 60 grating sensors was recently developed [22]. The system is schematically illustrated in Fig. 5. Single-mode optical fiber switches driven under PC control are utilized to allow the measurement of strain along 5 independent strings of 12 FBG sensors. The strings are illuminated using a single 1.3 μm ELED source ($\sim$150 μW power) through a 3 dB coupler and the switches. This processing occurs for each of the 60 elements in the array within a 2.5 s interval (with 50 averages/sensor), which is more than an adequate sampling rate for static strain monitoring, for example, in civil engineering. Obviously, by using a switch with more ports, a larger number of sensors could be monitored.

Fig. 6 shows the lab performance of the system. Here, all 60 sensors were monitored over a 30 minute period. Two sensors were strain-modulated to demonstrate the performance of the system. One with a 100-μstrain square wave modulation function at a period of $\sim$4 min, and the other with a sine-wave modulation of period $\sim$2 min. The short term resolution of the system was $\sim \pm 1$ μstrain, and drift over the 30 min period was $<\pm 3$ μstrain, which was attributed to slight temperature fluctuations in the laboratory.

The scanning optical filter approach has the drawback of utilizing only a narrow "slice" of the optical spectrum at a given time. When an array of FBG's, spanning a spectral range, is repeatedly interrogated at a frequency f, the amount

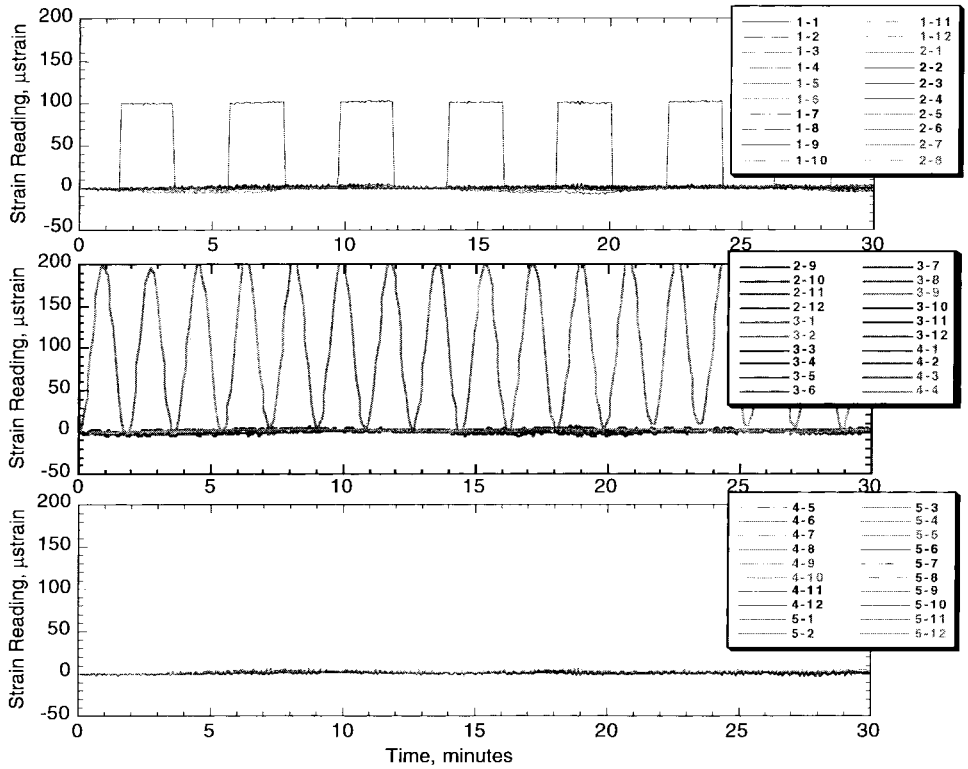

Fig. 6. Laboratory performance of the 60 channel FBG sensor system.

of energy E_R reflected by each FBG per sample period is equal to its reflectivity times the spectral brightness of the source times the grating's spectral width divided by the repetition frequency. When a scanning filter is used, the amount of energy available for detection is E_R times the filter's bandwith $\Delta\lambda_f$, divided by the width of the scanned wavelength range λ_s. As a result, if the filter's bandwidth equals $\sim$1% of the scanned width and each FBG is very strong (>95% reflecting), the detectable energy E_D per scan from each FBG is approximately $0.01E_R$. Consequently, relatively strong reflectors and/or bright sources are generally required for good resolution of wavelength shifts. Nevertheless, measurements made with FBG's of $\sim$2–4% reflectivity and erbium fiber sources with average optical powers in the 10 mW range have demonstrated $\sim$1 μstrain resolution using the scanning filter approach.

The optical throughput power penalty of a scanned filter, however, can be avoided through parallel detection of the entire spectrum with a linear-array detector such as a charge-coupled device (CCD). In such a system, wavelength discrimination is achieved with a fixed dispersive element (e.g., prism or grating) which converts wavelength into position along a line imaged onto an array of detector elements, as depicted in Fig. 7. Because the CCD spectrometer collects all the light returned by each FBG over the entire scan period [23], $E_D = E_R$, so a 1% FBG provides as much signal with parallel detection as does a 95% FBG with scanned detection. Parallel detection is then effective with either a much dimmer source, or much lower reflectance gratings.

The CCD spectrometer was developed for instrumenting wavelength-stepped FBG sensor arrays fabricated on-line as

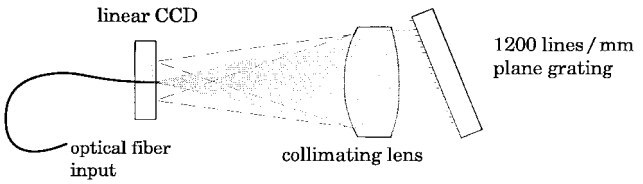

Fig. 7. Schematic of the fiber-coupled CCD spectrometer showing the CCD imager, collimating lens, and plane grating.

part of the fiber draw process [24]. Fig. 8 illustrates a typical array of gratings fabricated in this manner. The sensors are produced very rapidly (>1/s) and retain the original fiber strength (>5.5 GPa) since no handling of the bare glass occurs. While the single-pulse writing exposure results in reflectivities of <5% (@ 800 nm) for grating lengths below 1 cm, the CCD spectrometer readily detects reflections from these gratings, and provides high-speed strain information with moderate source intensities.

By dispersing a 24-nm bandwidth over a 256-pixel CCD, as many as 22 FBG's spaced by 1 nm may be resolved, with >0.4 nm overlap-free range (corresponding to a $\sim$600 μstrain range). The spectrometer's imaged wavelength dispersion is such that the center-to-center pixel spacing corresponds to $\sim$0.10 nm. Strain resolution of 1 μstrain requires a wavelength resolution of better than 0.0007 nm or less than 1/100th pixel. The image of each FBG is spread over several adjacent pixels, so a weighted average of the center wavelengths of those illuminated pixels λ_p scaled by each pixel's detected signal S_p gives the computed center of the reflected signal's wavelength

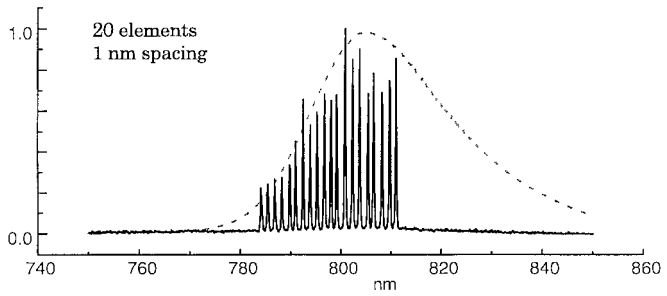

Fig. 8. Spectrum of 1–3% reflecting FBG's produced on the draw tower and detected with the CCD spectrometer at >3 kHz sampling rates. The shape of the source spectrum indicates the available range of the strain channels.

λ_B

$$\lambda_S = \frac{\sum(\lambda_p S_p)}{\sum \lambda_p}. \tag{5}$$

Strain sensitivity below 1 μstrain (without averaging) at repetition rates above 3.5 kHz has been demonstrated with 20 1–3% reflectors illuminated by several hundred microwatts of broadband light. As with other detection techniques, capacity can be expanded many times with a multiport fiber switch. CCD spectrometers adapted for strain measurement are much less developed than scanned detection methods, are only practical at wavelengths below 900 nm, and require bulk optics. However, parallel detection is insensitive to intensity and temperature fluctuations, and there is no time delay between channel readings. Along with its improved sensitivity, the advantages of parallel detection may be important in some applications.

The other form of direct spectroscopic tool for analyzing the return signals is analysis via Fourier transform spectroscopy (FTS). In this case, the light from an array of grating sensors is fed to an interferometer in which one arm can be scanned to change the relative optical path lengths. As the path difference passes through zero, a beat signal between the optical components is generated at the detector. For a multiwavelength signal, such as that produced by the grating array, the detector output comprises a series of discrete audio frequencies, each of which corresponds to a particular grating. Temperature or strain variations at a given grating modulate the corresponding frequency component.

An all-fiber scanning interferometer [25] has been demonstrated with a 30-cm optical path difference (OPD) scan capability for FTS analysis of gratings sensors. The system utilized a Michelson interferometer with Faraday-rotator mirrors as reflector elements to avoid unwanted polarization-induced fading of the interferogram [26]. Each fiber arm was approximately 100 m in length, with one arm wound on a fiber stretcher element used to induce strains on the order of 0.1%. This produced a $\sim$10 cm physical path change in the length of one arm, corresponding to an approximately 30 cm change in optical path length in the interferometer. Resolutions on the order of $\sim$0.015 nm were reported with this system.

Another recently developed demodulation scheme utilized the broadband, ultra-short pulses generated by a passively mode locked fiber laser [27]. Pulses generated from such lasers are typically a few picoseconds in duration, and as a consequence of self phase modulation, they can exhibit optical bandwidths in excess of 80 nm in the 1.55 mm window [28]. These pulses were injected into a long coil of highly dispersive fiber and then into an array of FBG's. The reflected pulses then traversed the dispersive coil a second time on their way to a high speed detector connected directly to a sampling oscilloscope. The highly dispersive fiber acts to form a passive wavelength-dependent optical delay line. Thus, in the time domain an array of FBG's would generate a sequence of pulses separated by the time of flight between gratings, plus a wavelength-dependent delay resulting from the double-pass through the highly dispersive fiber. For applications where the physical spacing L between gratings is effectively constant (i.e., for small εL), only changes in the Bragg wavelength will shift the relative time of the reflected pulses. Strain sensitivities of approximately 20 μstrain were demonstrated, limited by the total fiber dispersion of only -540 ps/nm, and the timing jitter of the oscilloscope. With a higher dispersion fiber or a long (approximately, 30 cm) chirped Bragg grating, it is believed that 1 μstrain sensitivities could be obtained by this method. The conventional, wavelength-domain demodulation is limited by the spectral separation between adjacent gratings, while time-domain demodulation lifts this restriction. As only the induced delay is measured, the wavelengths of different gratings may be allowed to shift past one another, or even overlap spectrally, so long as sufficient light is returned from each grating to determine the arrival time of its reflection. Finally, it should be noted that it should be possible to derive both the local strain *at* the individual elements and the integrated strain *between* elements by comparing a direct temporal interrogation (i.e., standard OTDR) with the dispersive OTDR result.

B. Time- and Wavelength-Division Multiplexing

A primary advantage of using FBG's for distributed sensing is that large numbers of sensors may be interrogated along a single fiber. WDM provides for tens of sensors per fiber, but time-division multiplexing (TDM) can multiply this number several times by re-using of the spectrum of the source. With mixed WDM/TDM in the serial configuration of Fig. 9(a), several wavelength-stepped arrays are concatenated, each at a greater distance along the fiber. By launching a short pulse of light from the source, the reflections from FBG's, at successively more distant positions along the fiber, will return to the detector at successively later times. The detection instrumentation is configured to respond to the reflected signals only during a selected window of time after the pulse is launched, so that a single WDM set of sensors is selected for detection.

This approach has been demonstrated using a 3×3 grating array with time-gating at the detector combined with the scanning FP filter wavelength detection [29]. Fig. 10 shows the outputs obtained with the nine element array: Here, a strain perturbation was applied to only one grating (#9), while the others were left unstrained. This approach has the potential to be expanded to much larger arrays, e.g., 10×10 for

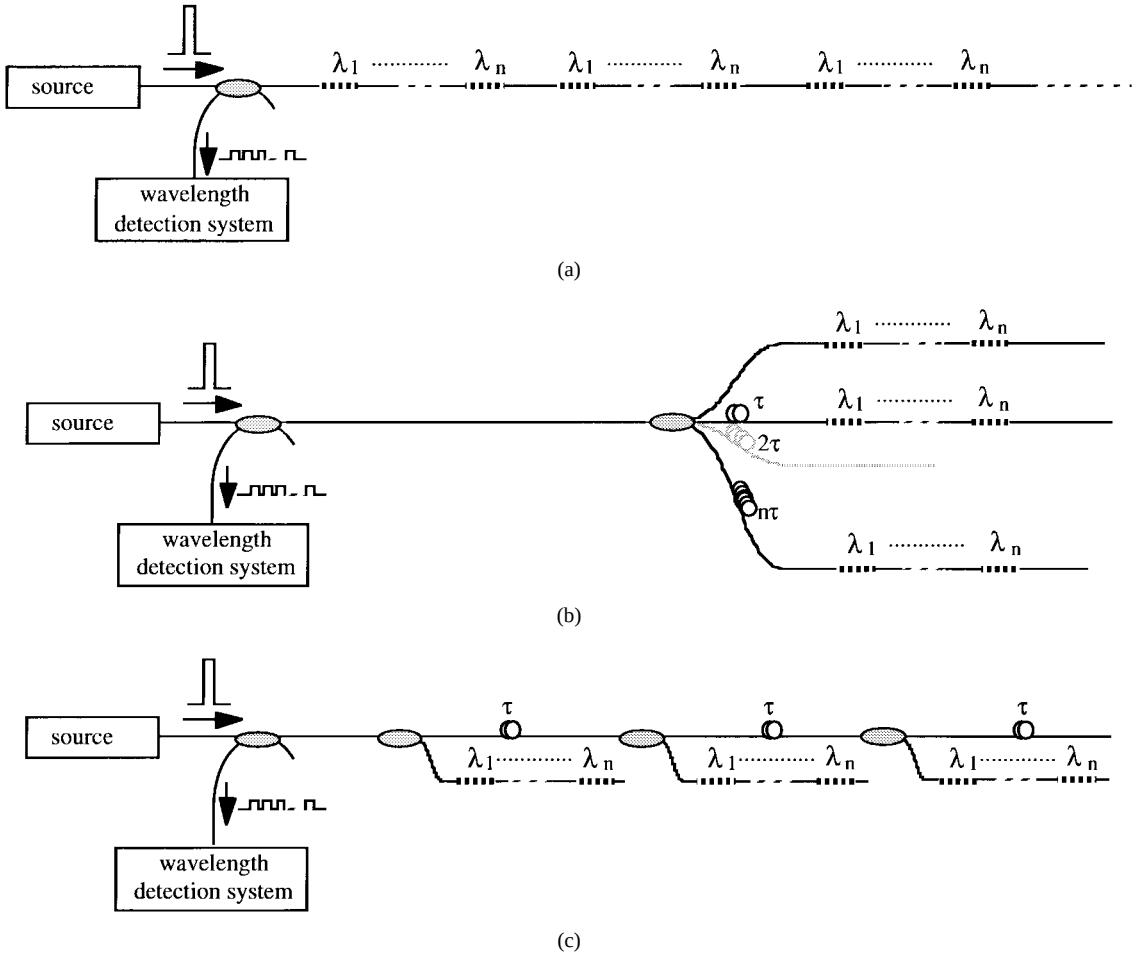

Fig. 9. WDM/TDM addressing topologies for FBG arrays. (a) Serial system with low reflectivity gratings, (b) parallel network, and (c) branching network.

example for a 100-element system would be feasible with current components.

Although TDM with CCD detection has not yet been demonstrated, the pairing of low-reflectivity gratings with high-sensitivity detection will be critical to interrogating large numbers of FBG's in a single fiber [Fig. 9(a)] because of two deleterious effects that can arise with strong reflectors. FBG's whose reflected light signals are separated in time, but which overlap in wavelength can experience cross-talk through what can be termed "multiple-reflection" and "spectral-shadowing."

Multiple-reflection crosstalk arises due to light reflected from one grating which arrives in the time window allotted to the detection of a downstream grating, because multiple reflection paths have delayed some of the first grating's signal. The analysis of this problem is nearly identical to that covered in [76]. The effect is, obviously, strongly dependent on the reflectivity of the gratings, and can be minimized by the use of low reflectivity gratings.

Spectral-shadowing crosstalk is defined as distortion of a downstream FBG's spectrum due light having to pass twice through an upstream FBG. If the two gratings' center wavelengths are slightly offset, it appears as though the downstream FBG is shifted further in the direction of the actual offset. The worst case distortion, with two FBG's equal in width and reflectivity, occurs approximately when they are spectrally offset by their FWHM. The error will vary somewhat with the detection method, but errors >1 μstrain are projected for a pair of interfering FBG's with reflectivities $>5\%$ [23].

The TDM/WDM parallel and branching optical fiber network topologies of Fig. 9(b) and (c) eliminate these deleterious effects, but at the price of reduced overall optical efficiency and the need for additional couplers and stronger FBG's.

C. Dynamic Strain Sensing

The use of interferometric configurations to detect the shift in the resonance condition of a Bragg grating have been described by a several groups [30]–[32]. An unbalanced interferometer is an optical filter element with a transfer function of the form $\{1 + \cos \phi\}$ where the phase term depends on the input wavelength. Fig. 11 shows the general principle of this technique applied to grating sensors. Light reflected from a grating is directed through an interferometer which has unequal paths. Due to the inherent wavelength dependence of the phase of an unbalanced interferometer on the input wavelength, shifts in Bragg wavelength are converted into phase shifts. One caveat with this approach is that the interferometer path difference must be kept less than the effective coherence length of the light reflected from the grating ($\sim$1 cm for a 1-cm grating @ 1.3 μm). As

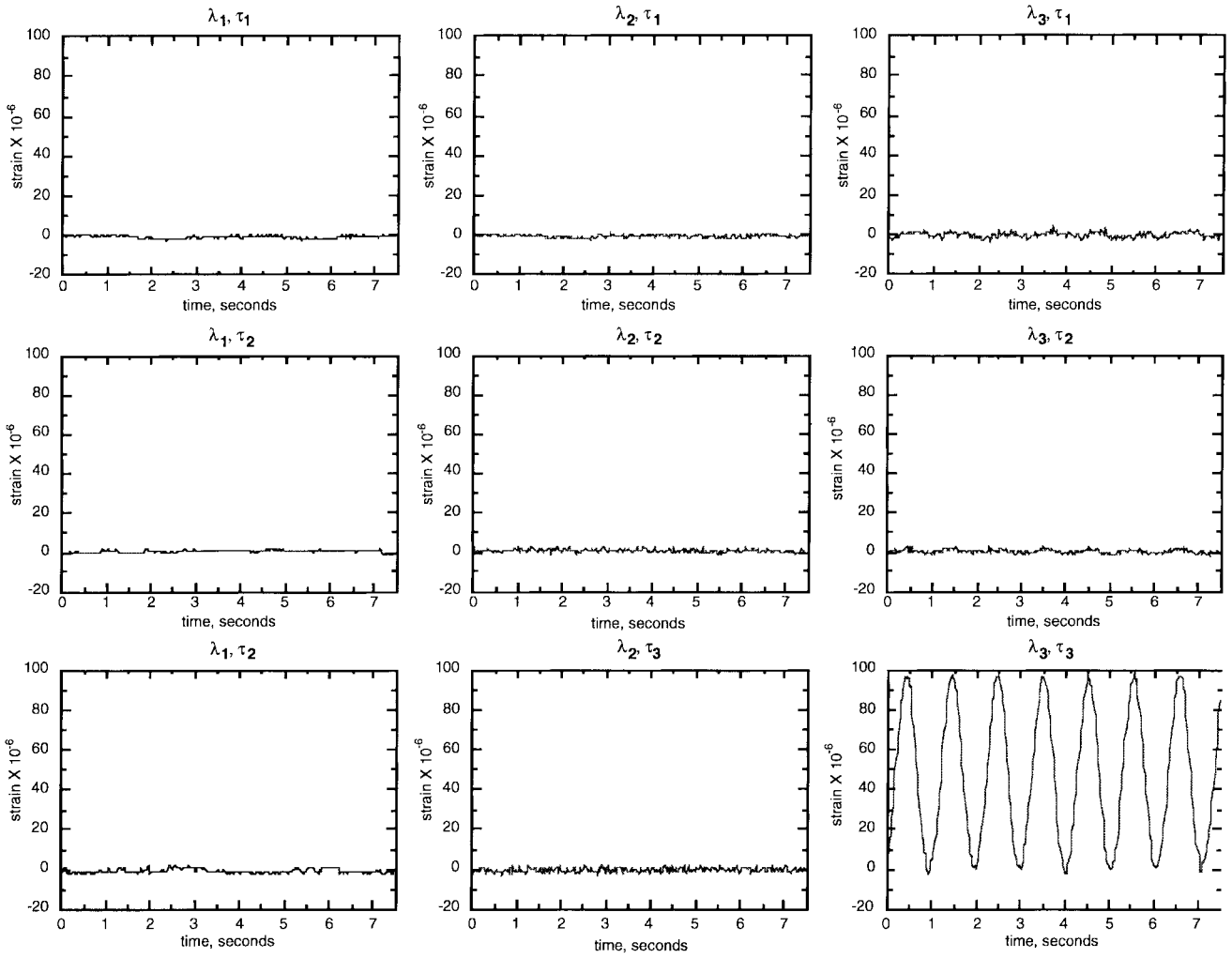

Fig. 10. WDM/TDM system outputs for a 3 × 3 array.

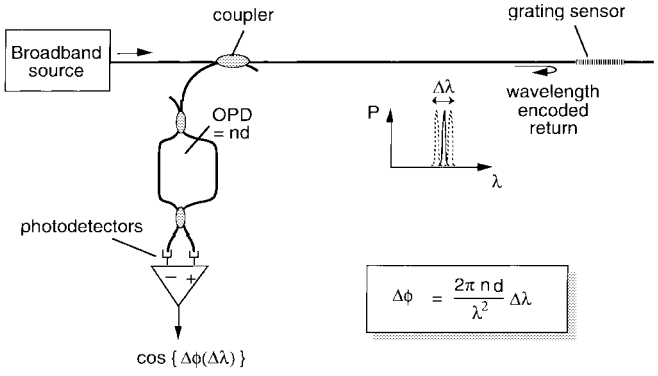

Fig. 11. Interferometric detection system for FBG sensors.

the interferometer output can be modulated via control of the path imbalance between the interferometer arms, various phase-reading techniques can be applied to determine phase modulation, $\Delta\phi$, induced by FBG wavelength shifts, $\Delta\lambda$.

The dependence of the output phase change on Bragg grating wavelength shift is given by

$$\Delta\phi = \frac{2\pi nd}{\lambda^2}\,\Delta\lambda. \tag{6}$$

By appropriate choice of the interferometer OPD ($= nd$), this technique can be made to be extremely sensitive to weak dynamic Bragg wavelength shifts: For example, with an interferometer of OPD of 1 cm (∼6.7 mm fiber length) the output wavelength-to-phase conversion factor is ∼37 rad/nm at a wavelength of 1.3 μm. Using the grating strain response of approximation 1 nm/1000 μstrain (at 1.3 μm), the strain-to-phase response of the system is ∼0.037 rad/μstrain. Typically, with interferometric systems, measurements down to μrad/$\sqrt{\text{Hz}}$ levels are possible, which results in predicted strain resolution of ∼0.035 nanostrain/$\sqrt{\text{Hz}}$ (35 picostrain/$\sqrt{\text{Hz}}$). Although this sensitivity has yet to be demonstrated, a sensor with a resolution of 0.6 nanostrain/$\sqrt{\text{Hz}}$ has been demonstrated. It is interesting to note that the equivalent wavelength shift corresponding to this strain change is on the order of $\sim 10^{-6}$ nm at 1.3 μm (or ∼100 kHz shift in optical frequency).

Although very sensitive to dynamic strains, the interferometric technique can be problematic when used for quasistatic strain measurements due to drifts in the interferometer bias phase itself. This can lead to inaccurate readings. However, a technique to compensate for this drift using a reference wavelength to directly monitor the interferometer stability has been reported [31]. This approach has been used to improve

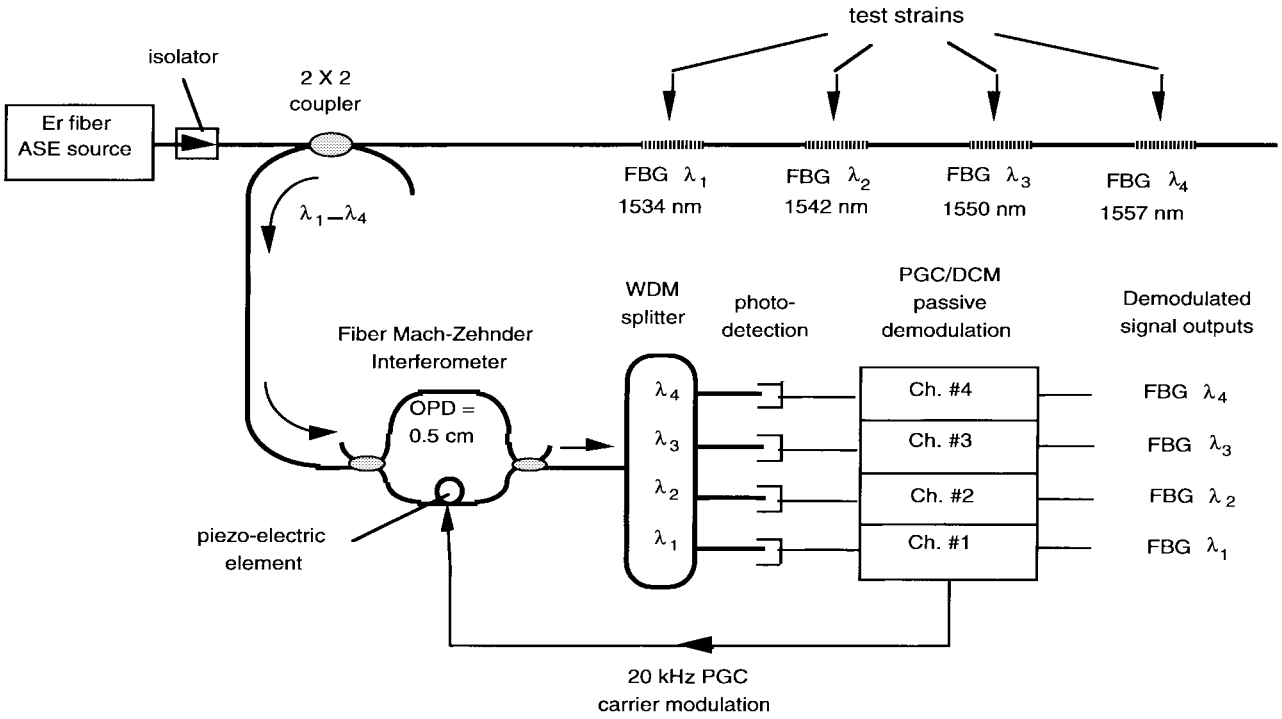

Fig. 12. Multiplexing system for interferometric detection using a four-channel WDM splitter.

the ability of FBG's to monitor temperature, and in particular to allow differential temperature measurements [32].

Multiplexing using the interferometric detection system has been demonstrated via the use of both wavelength- and time-division based addressing techniques. In the case of TDM addressing, the multiplexing of 8 gratings sensors was demonstrated using a pulsed optical source and a single "read-out" interferometer [33]. In the case of WDM addressing, wavelength demultiplexing filters have been used to separate the outputs from an array of gratings after they pass through a single interferometer [34]. The system is illustrated in Fig. 12. Here, four Bragg gratings at wavelengths of 1.535, 1.542, 1.549, and 1.56 μm were interrogated using an Er-doped fiber amplified spontaneous emission (ASE) source. The optical returns from the gratings were directed through an unbalanced interferometer followed by a four-port wavelength division demultiplexer, which directed the component at each wavelength to separate detectors. Each of these outputs is an interferometric output of the form previously described. Phase detection can be accomplished for each of the four wavelengths, $\lambda_1 \cdots \lambda_4$, by utilizing phase generated carrier demodulation simultaneously applied to each interferometer signal by a p/z fiber stretcher in one arm of the interferometer. Noise-equivalent sensitivities of $\sim$1.5 nano-strain/$\sqrt{\text{Hz}}$ were reported with the system. This approach can be extended to 8 or 16 wavelengths using currently available components, and is also suitable for use with the TDM/WDM topologies of Fig. 9.

D. Temperature/Strain Discrimination

One of the most significant limitations of FBG sensors is their dual sensitivity to temperature and strain. This creates a problem for sensor systems designed to monitor strain, as temperature variations along the fiber path can lead to anomalous, thermal-apparent strain readings. One approach to addressing this issue is to use reference gratings along the array, i.e., gratings that are in thermal contact with the structure, but do not respond to local strain changes. This technique provides some compensation, but a system capable of providing strain and temperature measurements from the same fiber without requiring that a section of the fiber be isolated from strain is much more desirable. One approach is to locate two sensor elements which have very different responses to strain ($K_{\varepsilon 1}$, $K_{\varepsilon 2}$) and temperature (K_{T1}, K_{T2}) at the same point on the structure (collocated sensors). Then a matrix equation

$$\begin{pmatrix} \Delta\lambda_1 \\ \Delta\lambda_2 \end{pmatrix} = \begin{pmatrix} K_{\varepsilon 1} & K_{T1} \\ K_{\varepsilon 2} & K_{T2} \end{pmatrix} \begin{pmatrix} \varepsilon \\ T \end{pmatrix} \tag{7}$$

can be written and inverted to yield strain and temperature from measurements of the two wavelength shifts. The success of this technique depends on the ratio of the strain responses of the two sensors being different from the ratio of their temperature responses, so that the determinant of the matrix is nonzero. For FBG's, the wavelength dependence of the photoelastic and thermooptic coefficients of the fiber glass cause a small variation in the ratio of responses of FBG's written at different wavelengths. Xu *et al.* [35] measured the responses of a collocated 850 and 1300 nm pair of FBG's, and found that the responses were 6.5% higher for strain and 9.8% less for temperature at 1300 nm compared to 850 nm. These researchers concluded that this approach has the potential for simultaneously determining strain and temperature to ± 5 °C and ± 10 μstrain. Other types of fiber gratings, such as rocking filters and long-period gratings (discussed later in

this review), can have very different responses from FBG's even if the two devices operate in the same wavelength band. Kanellopoulos *et al.* [36] reported simultaneous strain and temperature measurement using an FBG and a long period rocking filter in the 800 nm band, and obtained errors of ± 165 μstrain and ± 1.5 °C. We have demonstrated that a long-period grating and FBG's in the 1300 nm band can be used to determine strain and temperature to ± 9 μstrain and ± 1.5 °C. Assuming improved resolutions can be attained, this technique could provide a practical means for providing strain/temperature discrimination in arrays of grating sensors. This approach is described in more detail later in the paper.

III. Chirped Grating Sensors

The majority of sensing techniques based on gratings utilizes only the most basic properties of FBGs; namely the wavelength-encoded nature of the devices. More novel sensors based on chirped and other tailored grating structures are, however, possible, and several examples have been reported in the literature.

Interest in chirped gratings focused originally on their potential for dispersion compensation in high bit-rate telecommunications systems [37]. Several techniques for fabricating chirped Bragg gratings were demonstrated. Until recently chirped fiber Bragg gratings proved inadequate for their intended purpose.[1] However, as it often happens in technology, ideas in one arena find applicability in another. Specifically, the types of gratings originally designed for dispersion compensation needed only slight modification to be useful in the development of a new brand of strain and temperature sensors.

Since a chirp is achieved simply by varying the grating period, the average index, or both along the length of the grating, the method chosen for making a chirped grating must target one or both of these free parameters. Byron *et al.* first demonstrated a method for making chirped gratings by tapering a fiber in the region of the grating [38]. The decreasing core size decreases the effective index along the length of the taper, resulting in a chirp. This technique, though well-suited for relatively small chirps (<3 nm), requires fairly extreme tapers (decrease in OD from 125 to 50 mm) to achieve even moderate chirps (>3 nm), and the small core diameters result in increased susceptibility to bend loss.

An alternative method, demonstrated by Hill *et al.*, involves bonding an unchirped grating to a substrate with a "soft glue" that allows a strain gradient to be formed along the grating length through the differential shear strength of the glue [39]. This technique allows dynamic control of both the spectral shape and location of the grating after fabrication. However, it is not generally compatible with the requirements of many sensing applications which often involves embeddment of the sensor in materials like concrete or composites.

[1] Chirped fiber Bragg gratings have now been fabricated up to one meter in length with the appropriate dispersion needed for compensating high bit-rate transmission of pulses at 15.5 μm in fiber originally designed for 1.3 μ application.

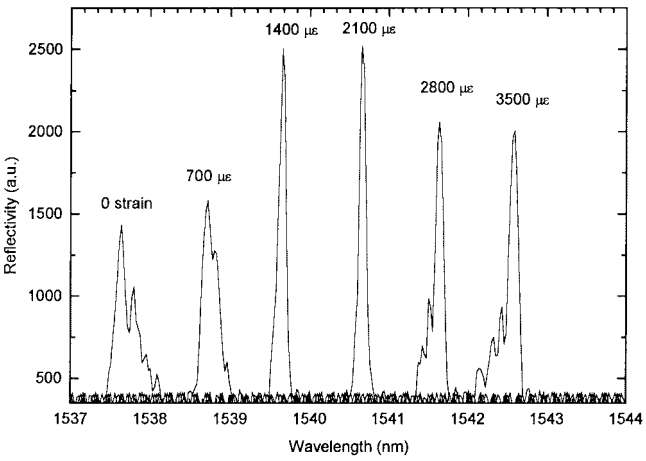

Fig. 13. Reflectance spectra of chirped grating tapered from 115 to 105 μm before grating under ~ 1700 $\mu\varepsilon$ and measured under different strains.

A. Tapered Grating Sensor

We reported on the fabrication and properties of a chirped grating which capitalizes on the strain gradient realized when a tapered fiber is under tension [40]. Only the outer diameter of the fiber is tapered in the region of the grating, eliminating effects associated with changing the effective index, while allowing control over the spectral shape and location of the chirp. The chirped gratings were fabricated in hydrogen loaded, Ge-doped silica fibers and exposed with a KrF excimer laser. The fibers were held under preset tension during exposure while in contact with the phase mask. The tapers were fabricated by lowering a section of fiber into a buffered HF solution at a constant rate (20 mm/h) using a computer-controlled translation stage. Various linear tapers were made, ranging from 115 $\rightarrow$ 85 mm to 115 $\rightarrow$ 105 mm by adjusting the rate of submersion and the acid strength. Because the etch rate is linear with time, controlled and reproducible taper profiles were easily achieved. Though the tapers used in this study were linear, the process can be generalized to fabricate higher order tapers as well, by varying the immersion rate.

Fig. 13 shows a series of spectra taken from a 115 $\rightarrow$ 105 μm chirped grating (where the two numbers refer to original and minimum diameter of the etched taper). In this case, the fiber was first tapered, and then the grating was written while the fiber was subjected to a 1750 $\mu\varepsilon$ tensile load. After removal from the exposure mount, the grating was analyzed with a scanning erbium fiber laser under six different loads from 0 to 3500 μstrain. As seen from the results, the unstrained fiber contains a chirped grating. Subsequent strain causes the reflectance peak to narrow and shift until the tension at which the grating was exposed is applied; at this point the width and location are now the same as that of an untapered fiber exposed under zero strain. Additional strain causes it to shift further, and broaden.

The strain profile along the length of the taper can be calculated point-by-point from

$$\varepsilon_i = \varepsilon_{i-1} \frac{A_{i-1}}{A_i} \tag{8}$$

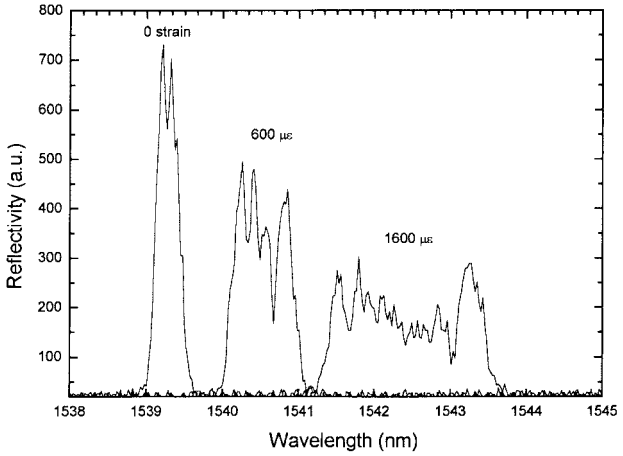

Fig. 14. Reflectance spectra of chirped grating tapered from 115 to 85 μm after grating writing under zero strain and measured under different strains.

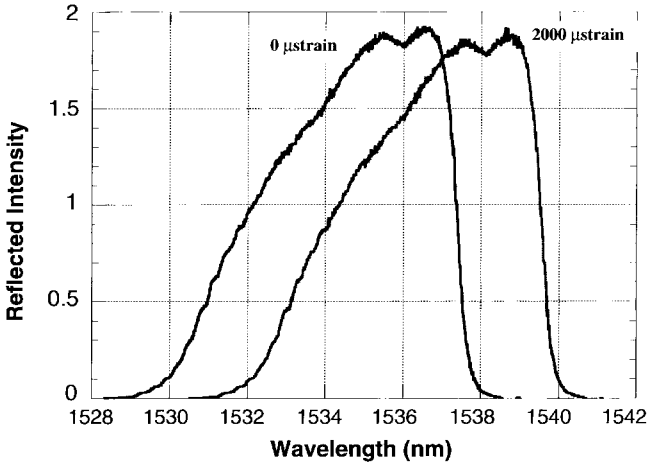

Fig. 15. Spectrum of the asymmetric profile FBG at 0 and 2000 μstrain (resolution = 0.2 nm).

where ε_i and A_i are the strain and cross-sectional fiber area at the point i. Based on the diameter differences and the applied strain of 1750 $\mu\varepsilon$, a chirp of 0.4 nm is calculated for this grating, which agrees well with the experimental results shown in Fig. 13.

We have also fabricated chirped Bragg gratings by exposing an untapered fiber then etching it in a more concentrated HF solution, which produced a linear taper from 115 to 85 μm over a 20-mm long section. As seen in Fig. 14, fabricating the grating in this manner results in a narrow-line grating in the unstrained fiber. An applied strain then results in spectral broadening and a shift in the peak of the spectrum. The more pronounced chirp per unit applied strain, evident in Fig. 14, is a consequence of the more pronounced taper.

Such devices behave uniquely in the presence of strain and temperature fields. Their response to strain results in a broadening and a shift in the Bragg condition, while temperature effects only the location of the centroid through the temperature dependent index of refraction (dn/dT). By carefully calibrating and simultaneously measuring the spectral shift and broadening, in principle one can use such devices to simultaneously measure strain and temperature [40].

B. Reflectometric Chirped-Grating Sensor

Another example of the use of a chirped fiber Bragg grating sensing element is to utilize a grating with an asymmetric broadband spectral response as a strain sensitive reflective filter [41]. A measure of the strain applied to the grating is obtained from the reflectivity of the grating at a particular probe wavelength. This concept is particularly suitable for use with simple optical time domain reflectometry addressing a large number of such weakly reflecting gratings.

In this instrumentation approach, a narrowband source is used in conjunction with a broadband sensor grating element. Strain induced shifts in the spectrum of the grating then result in a changes in the reflectivity of the device as measured at the source wavelength. The type of grating which can be used for this technique can be either a simple broadband grating formed by a constant pitch short grating; e.g., a grating of length $\sim$50 μm produces a BW of $\sim$3 nm at 1.3 μm, or a tailored device in which the pitch is chirped to produce a broadband response, and apodization is used to modify the spectral response. One type of device which might be particularly suitable for this type of application is a strongly asymmetric device with a "ramp" type of spectral profile providing a gradual change in reflectivity along one edge of the response. For a probe wavelength corresponding to the mid point of the long-edge region of the asymmetric grating response, compressive or tensile strain applied to the grating gives rise to either increasing or reduced reflectivity. Via the use of OTDR interrogation the reflection coefficient of a series of such weakly reflecting gratings at multiple spatial locations along the fiber could be assessed, allowing distributed sensing capabilities.

Fig. 15 shows the spectrum of a chirped and strongly apodized grating fabricated using a phase mask with a curved fiber in the plane of the mask, as described by Sugden *et al.* [42]. Curving the fiber has two effects in this process: first, a chirp is created by fiber geometry, and second, a strong asymmetrical apodization of the grating coupling strength occurs along its length. This latter effect arises due to both the reduction in the efficiency of the grating sections with increasing blaze angle, and the fact that the curved-fiber geometry means that a uniform exposure is not attained along the entire length.

Fig. 15 also demonstrates the shift of the profile with strain (2000 μstrain). As observed, the profile retains its asymmetrical form, and the peak wavelength shift is in good agreement with the expected shift. Fig. 16 illustrates the change in reflectivity with strain applied to the grating for a probe wavelength of 1534 nm.

With a series of weak asymmetric gratings, OTDR interrogation could be used to accurately monitor the reflection coefficient at multiple points along the fiber providing a distributed sensing capability. In this case, the OTDR background (scattering) could be used as a reference to reduce the effects of extraneous losses. This type of grating could also be utilized as the primary sensing element for a variety of discrete sensors. For example, using the device as part of a pressure sensing probe in which the pressure alters the strain on the grating

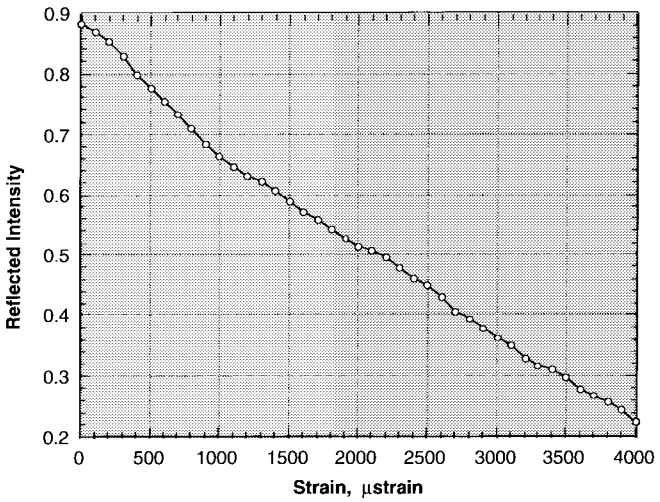

Fig. 16. Change in reflectivity of the asymmetric FBG at a fixed "probe" wavelength of 1534 nm.

could yield a simple sensor in which the reflectivity is a direct function of the pressure.

C. Intragrating Sensing

The changes in the reflection spectrum caused by a nonuniform measurand field along the length of a grating forms the basis of a relatively recent and potentially powerful technique called intragrating sensing. This approach involves detailed analysis of the reflection spectrum in order to obtain a continuous profile of the measurand over the length of the grating. Profiles of grating lengths ranging from 5 mm to 10 cm have been reported [43]–[47], with a spatial resolution as low as 0.4 mm [43]. This technique exploits the fact that different sections of the grating will contribute to the reflection at different wavelengths when the gratings modulation periodicity is nonuniform along its length. Each section of the grating can be considered to mainly contribute at the "local" Bragg wavelength given by

$$\lambda_B(z) = 2n(z)\Lambda(z). \tag{9}$$

Therefore, if a uniform grating (i.e., constant n and Λ) is subjected to a nonuniform strain $\varepsilon(z)$, or temperature $T(z)$ profile, different parts of the gratings will contribute to different wavelengths according to the local state of the measurand. As a consequence, its reflected spectrum will broaden, and the peak reflectivity will decrease. Both the intensity and phase response of the grating are affected by this nonuniformity. Analyzing either the intensity or the phase component of the reflection spectrum, or both, permits one to deduce $\lambda_B(z)$. The subtraction of $\lambda_B(z)$ from the "as-written" grating distribution $\lambda_B^0(z)$ yields $\Delta\lambda_B(z)$ from which either $\varepsilon(z)$ or $T(z)$ is obtained. If one starts with a uniform grating, the original $\lambda_B^0(z)$ profile is just the Bragg wavelength of the grating λ_B^0. There are, however, advantages associated with using an initially chirped grating, the simplest form being a linearly chirped grating such that $\lambda_B^0(z) = \lambda_B^0 + G(z - z_{\text{center}})$ where G is a constant and z_{center} is the position of the grating's center.

1) Intensity-Based Intragrating Sensing: The intensity-based analysis is the simplest intragrating sensing approach. Here, one needs only the intensity reflection spectrum $R(\lambda)$, obtained conventionally using an optical spectrum analyzer or a scanning FP filter as described earlier. The distribution $\lambda_B(z)$ is obtained as the solution of the following integral equation [43]:

$$\int_{\lambda[z=-(L/2)]}^{\lambda(z)} -\ln\left[1 - R(\lambda')\right] d\lambda' = \pm\frac{\pi^2}{2}\int_{-(L/2)}^{L/2} \frac{\Delta n^2(z')}{n(z)}\, dz'. \tag{10}$$

Here, $\Delta n(z)$ is the depth of modulation imposed on the grating by the writing UV beam. This indicates that the intensity-based approach requires detailed knowledge of the gratings' characteristics [specifically, $\Delta n(z)$]. A simplification of (10) comes when $\Delta n(z)$ is uniform; for increasing $\lambda(z)$, we get

$$z(\lambda) = -\frac{L}{2} + \frac{2n}{(\pi\Delta n)^2}\int_{\lambda[z=-(L/2)]}^{\lambda} -\ln\left[1 - R(\lambda')\right] d\lambda'. \tag{11}$$

We also have neglected the nonuniformity of n inside the right integral of (10). This is of no consequence here, given the fact that only small changes of n are involved. Note also that when $R(\lambda)$ is small, $-\ln\left[1 - R(\lambda)\right] \sim R(\lambda)$. A limitation of this approach is that only profiles which result in monotonic $\lambda_B(z)$ can be interpreted with the intensity technique. If we start with a uniform grating, this means that only strain or temperature profiles which are continuously increasing or decreasing along the grating, can be measured. In addition, the technique does not give the sign of the gradient [this is the reason for the $\pm$ sign in (10)]. In many situations, however, the sign of the strain gradient is known *a priori*, removing this limitation. Furthermore, if one uses an initially chirped grating, measurand fields which are nonmonotonic can be measured as long as the total effect of the measurand gradient is never large enough to cancel the pre-chirp bias of the grating. The use of a chirped grating also increases the spatial resolution of the measurement. This resolution is position-dependent and is given by [43]

$$\delta z(z) = \frac{1}{2}\sqrt{\frac{2n_0\Lambda_0^2}{\left|\dfrac{d\lambda_B(z)}{dz}\right|}}. \tag{12}$$

Figs. 17 and 18 depict an experiment that illustrates the use of the intensity approach. An initially chirped grating, about 19 mm long is used, and the temperature along the grating is the quantity measured. A small air jet is used to locally heat the optical fiber to a temperature around 70 °C over a very small length. The resulting temperature profile along the grating is nonuniform. As we can see from the bottom center-most graph in Fig. 16 the changes in $\lambda_B(z)$ are small compared to the initial chirp. However, it is clear from the spectrum and the calculation of $\Delta\lambda(z)$ that the change is clearly detected, and $T(z)$ has been evaluated with reasonable accuracy.

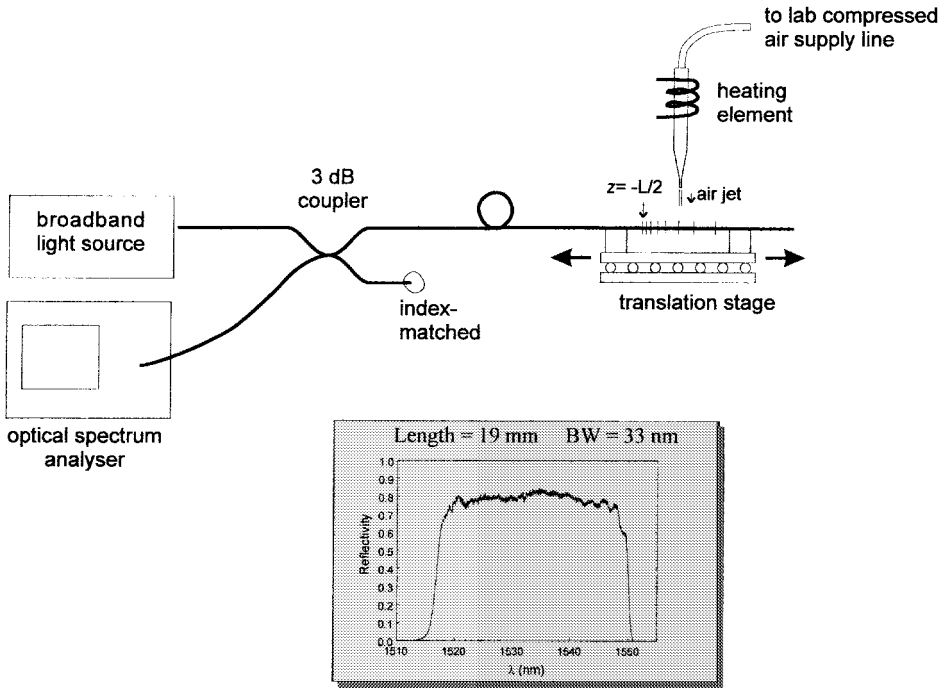

Fig. 17. Experimental arrangement for the intragrating interrogation of a grating. (The inset shows the measured original spectrum of the chirped grating used for this experiment.)

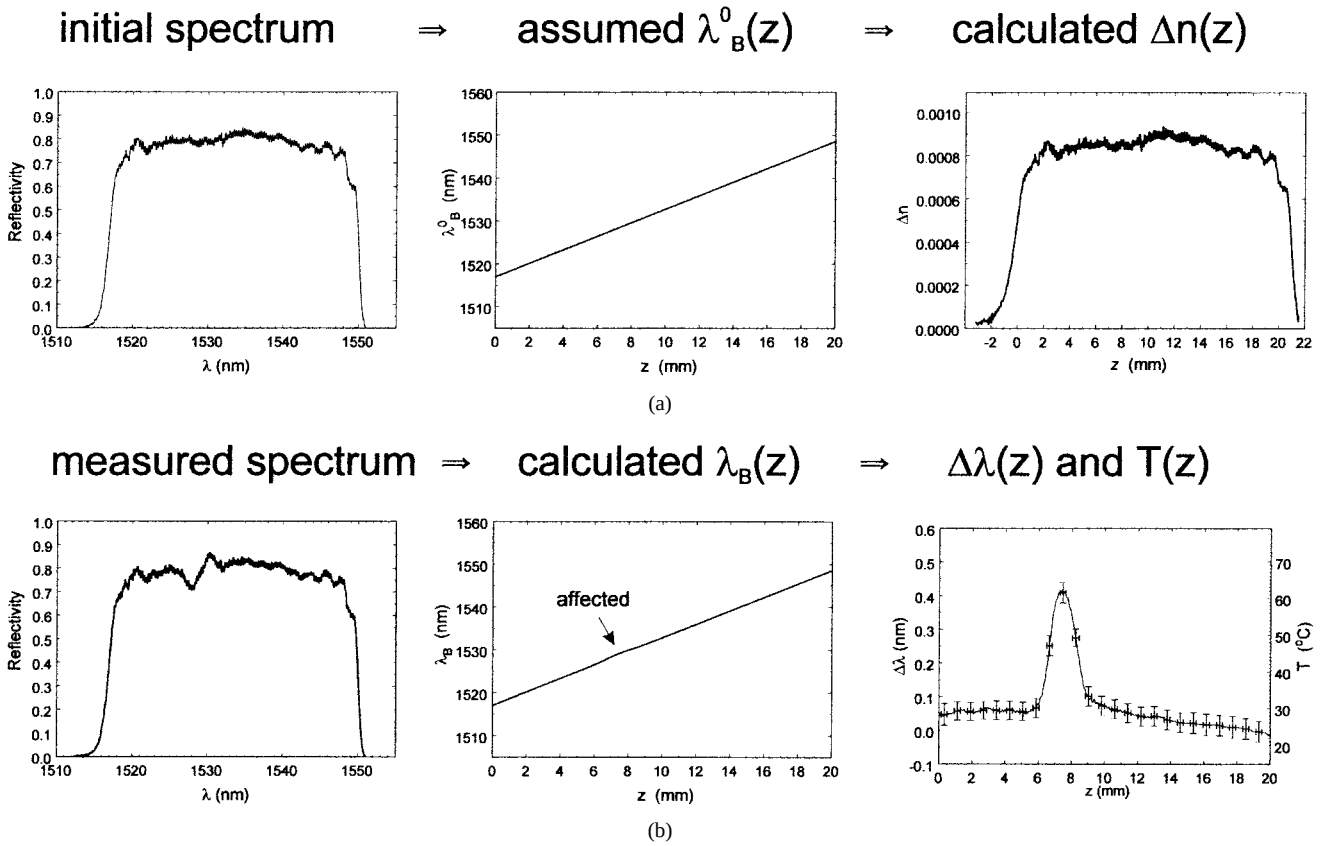

Fig. 18. Measurement of the sharp temperature profile increase due to the flow of a 1-mm diameter hot air jet over a section of a grating using the intensity-based Bragg intragrating sensing approach.

2) Phase-Based Intragrating Sensing: The phase response of the grating can be obtained using an arrangement such as the Michelson interferometer shown in Fig. 19. The theory for the conversion of the phase response to $\lambda_B(z)$, which is given by Huang *et al.* [47], is based on Ouellette's description of the dispersion in chirped fiber gratings [48]. The group delays

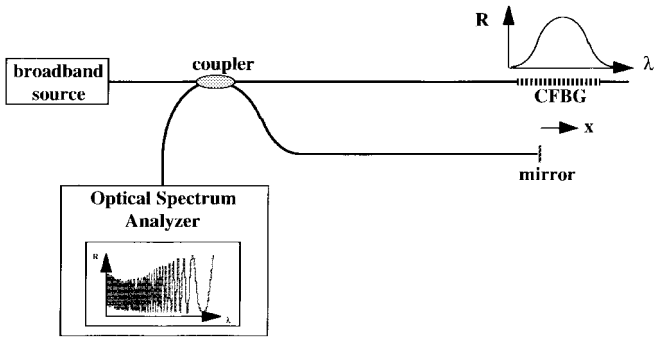

Fig. 19. Chirped grating fiber Michelson interferometer.

of the light propagating in the two interferometer arms will differ by an amount given by

$$\Delta\tau = \frac{\partial\phi}{\partial\omega} = \frac{2nz_P}{c} \tag{13}$$

where ϕ is the measured phase difference, $\omega = 2\pi c/\lambda$ is the angular frequency of the light, and z_p is the effective penetration depth, as measured relative to point along the sensing fiber where the optical path imbalance with the reference arm is zero. Expressed in terms of wavelength, we have

$$z_P(\lambda) = -\left(\frac{\lambda^2}{4\pi n}\right)\frac{\partial\phi}{\partial\lambda}. \tag{14}$$

(The dispersion of the optical fiber material is ignored in this result.) When the grating is monotonic and has a sufficiently large gradient (chirp), the center of reflection of light at a given wavelength is the point where the local Bragg condition (9) is satisfied; therefore, $z_p(\lambda)$ is just the inverse of $\lambda_B(z)$. An advantage of the phase-based approach compared to the intensity approach is that the sign of the gradient can be unambiguously determined. Another advantage is that one does not need to know $\Delta n(z)$ with a high degree of accuracy, as long as it is sufficiently high and varies relatively smoothly so that its variation does not affect the phase of the reflected light.

Fig. 20(a) shows the direct interferometric response of a chirped grating Michelson interferometer [49] of the form shown in Fig. 19. The system, in this case, used a grating 19 mm in length, 33 nm bandwidth centered at 1535 nm (similar to the one used in the previous example, see inset in Fig. 17). The interferometer arms were balanced in length at a point approximately 80% along the length of the chirped grating. The phase response was measured using broadband illumination from an erbium doped fiber ASE source and a scanning optical spectrometer. Fig. 20(b) shows the change in phase with wavelength derived from the raw interferometric response. Note that the density of fringes observed at the shorter wavelengths was beyond the resolution of our instrument, and therefore that part of the grating was excluded from the presented data.

The derivative of the phase plot of Fig. 20(b) is proportional to the group delay of the grating, and is shown in Fig. 21(a). The variation of the group delay with wavelength allows

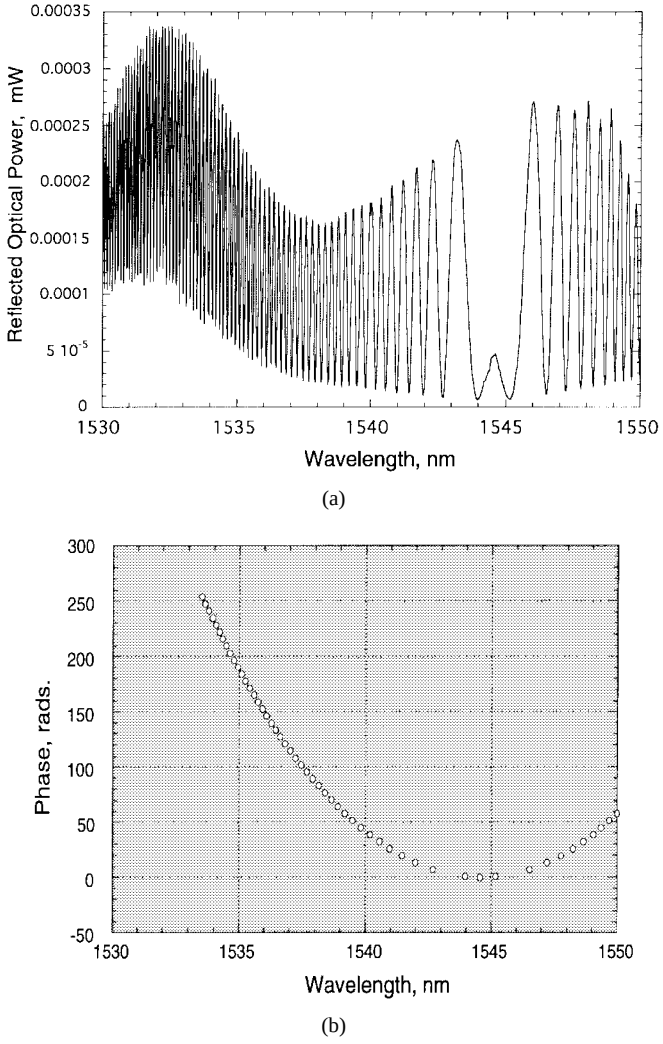

Fig. 20. Interferometer phase response (a) direct spectral output and (b) phase versus wavelength.

the relationship between the Bragg wavelength and spatial position along the grating (relative to the OPD balance point) to be determined through (14). This transformation of the data in Fig. 21(a) is shown in Fig. 21(b) for the "as-is" chirped grating, and clearly indicates a linear change in Bragg wavelength along the length of the grating. Fig. 21(c) and (d) show the same type of plots, but derived for the situation where the grating was subjected to a thermal gradient over a ~2 mm section near its center induced by placing the grating between two peltier elements separated by 2 mm at their edges. The deviation in the chirp characteristics created by the additional thermally induced chirp is clearly observed, illustrating the ability of the technique to assess the variation of the Bragg wavelength along the length of the grating.

3) Combined Intensity and Phase Measurement: When the reflectivity of the grating is low, its intensity and phase response are essentially equivalent to the Fourier transform (in the optical wavelength domain) of the grating's structure (in the spatial domain) [50]. Huang *et al.* have recently shown that this knowledge allows the determination of an arbitrary measurand profile based on the combined measurement of phase and intensity [47]. This approach removes the limitation

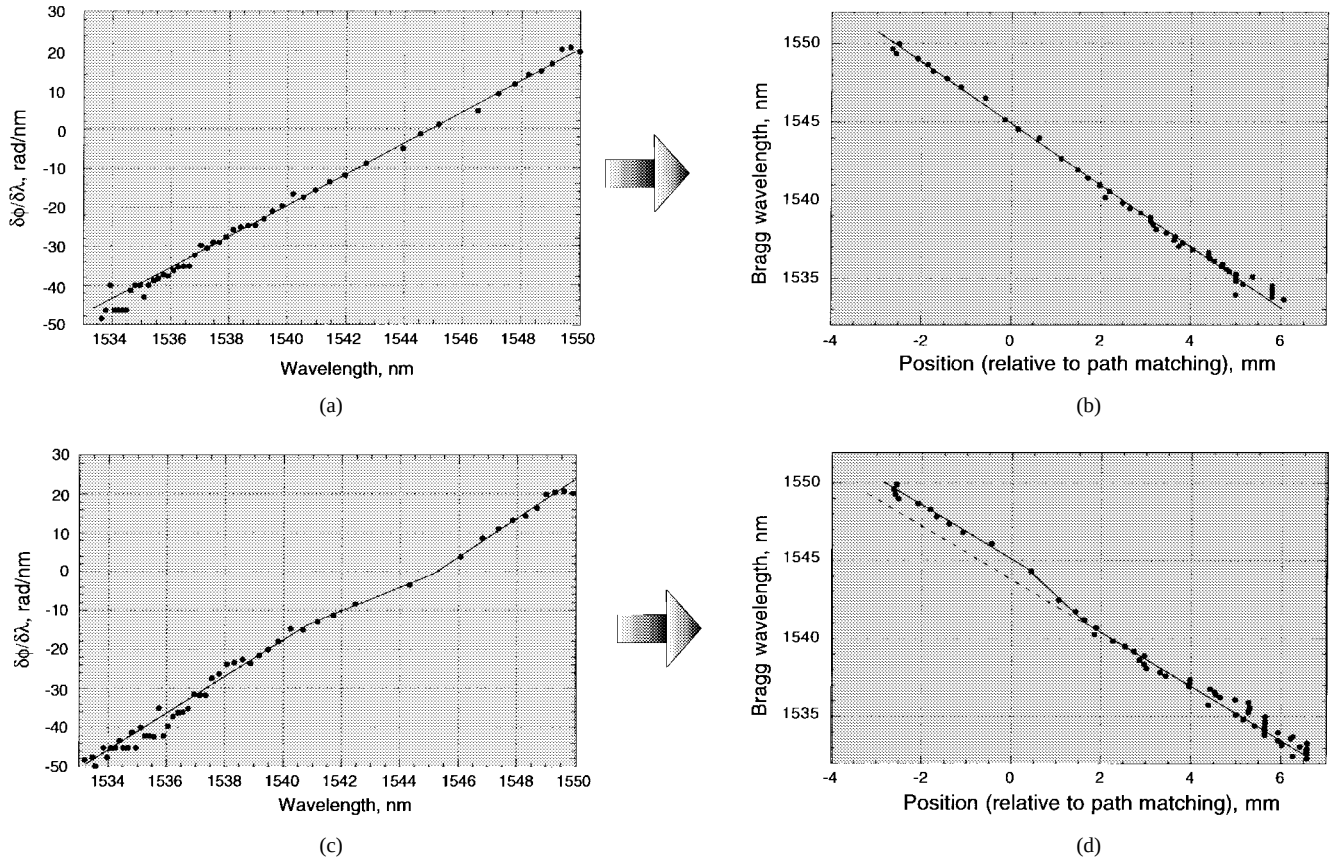

Fig. 21. (a) $\delta\phi/\delta\lambda$ for the "as-is" chirped grating and (b) variation in Bragg wavelength with spatial position along the grating derived from (a). (c) and (d) are the same plots as in (a) and (b), but with a thermally induced gradient over a $\sim$2-mm section of fiber near the center of the grating.

of monotonicity of the fields and allows, at least in principle, a spatial resolution not limited by the effective length. This presents a more complex operation because the set-up is slightly more involved, to measure both phase and intensity simultaneously, and more processing of the data is required. A full analysis of this new approach has yet to be performed, and at this stage it is not clear which of the interrogation approaches described would prove most useful for practical applications.

4) Low-Coherence Approaches: Volanthen *et al.* [51] have used another approach to obtain distributed strain measurement along a grating. Their set-up is similar to that of Fig. 19, except that the reference arm uses a grating as the reflector, which can be strained to make the reference reflector wavelength-tunable. A stretcher was attached to the reference arm so as to permit a scanning of the OPD of the interferometer. Finally, a piezoelectric actuator was used to generate a modulation of the OPD. All this is done to generate a rapidly changing optical signal at the detector which has peak amplitude when the OPD of the interferometer is optimized for the wavelength selected by the reference grating. In this way, a plot of optimal wavelength versus OPD is obtained, which gives, in essence, $\lambda_B(z)$. Low-coherence approaches to characterizing FBG's along their length have also been developed [52].

IV. Long Period Grating Sensors

In 1995, Vengsarkar *et al.* [53] introduced a new type of fiber grating device to the optics community. The long-period fiber grating, or LPG, is a periodic modulation of the core index of refraction written into a single mode fiber using UV exposure through an amplitude mask. A typical LPG has a period Λ in the hundreds of microns, a length of about 1–3 cm, and an index modulation depth of 10^{-4} or greater. The LPG couples light out of the core and into the cladding at specific wavelengths

$$\lambda_i = [n_{01} - n_{\text{clad}}^{(i)}]\Lambda \tag{15}$$

where n_{01} is the effective index of the core mode, and $n_{\text{clad}}^{(i)}$ is the effective index of the ith axially symmetric cladding mode. The light in the cladding quickly decays due to losses at the cladding/air interface, leaving a series of loss bands or resonances in the guided mode. Because $n_{\text{clad}}^{(i)}$ depends on the index of the medium surrounding the cladding, the section of the fiber where the grating is located is usually left stripped of its polymer coating after fabrication. An individual grating can have many resonances over a broad wavelength range, as illustrated by the transmission spectrum shown in Fig. 22.

LPG's were initially developed for use as band-rejection filters [54], and have been used for gain-flattening of erbium-doped fiber amplifiers (EDFA's) [55]. However, LPG's also present unique opportunities as fiber optic sensors. The center wavelengths of the LPG resonances depend critically on the index difference between the core and the cladding, and hence any variation caused by strain, temperature, or changes in the external refractive index can cause large wavelength shifts in the resonances.

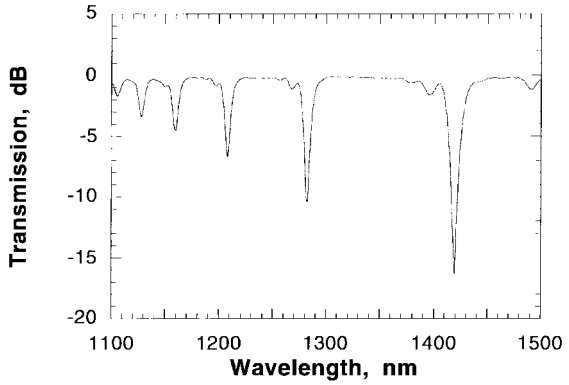

Fig. 22. Transmission spectrum of an LPG. Grating written in AT&T DSF fiber $\Lambda = 225$ μm.

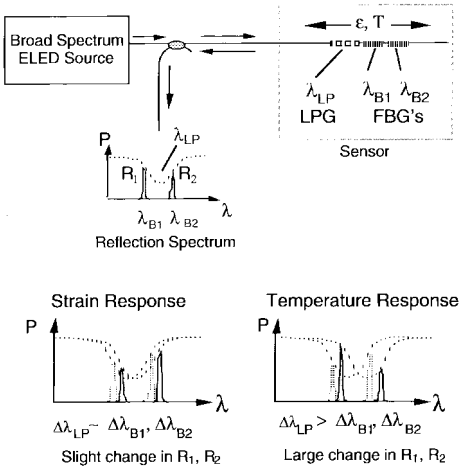

Fig. 23. Schematic of hybrid FBG/LPG sensor for simultaneous strain and temperature measurement.

For strain and temperature sensing, LPG's are unique among fiber grating sensors in that an LPG resonance at a given wavelength λ can have a very different sensitivity, depending on the fiber type and the grating period. The strain and temperature response of a long period grating resonance can be either positive or negative, depending on the differential responses of the core and cladding [56]–[62].

We have observed an LPG resonance with a temperature response as low as -0.20 nm/°C, and positive response as large as 0.15 nm/°C has been reported [56]. Observed strain responses range from -0.0007 to 0.0015 nm/$\mu\varepsilon$ [53]. Additionally, the responses of two resonance bands of the same LPG usually differ in magnitude. These properties make LPG's particularly useful for multi-parameter sensors such as the strain and temperature sensors discussed earlier. Two LPG resonances can be used to simultaneously determine strain and temperature using a single grating element, or an LPG resonance can be paired with an FBG to make the same measurement.

Fig. 23 shows the configuration of a hybrid FBG/LPG sensor which has been used to simultaneously determine strain and temperature at the sensing element using this technique [57]. The sensor consists of three gratings, an LPG with a resonance located at a wavelength λ_{LP} of 1306 nm, and two FBG's, with center wavelengths at $\lambda_{b1} = 1293$ nm and $\lambda_{b2} = 1321$ nm. In this system, the shift observed in the LPG wavelength with temperature was seven times that of the FBG's, while the strain response was about 50% that of the FBG's.

The sensor configuration uses the reflections of the two FBG's (R_1 and R_2) to interrogate the wavelength shift of the LPG resonance. For the initial demonstration, the wavelength shift of one of the FBG's and the change in the intensities of R_1 and R_2 were monitored using an optical spectrum analyzer. A change in strain leads to a small decrease in R_1 and small increase in R_2 because the shift in λ_{LP} lags the shift in λ_{b1} and λ_{b2}. However, a change in temperature produces a large increase in R_1 and large decrease in R_2, because the shift in λ_{LP} is much larger than the shifts in λ_{b1} and λ_{b2}.

The sensor was calibrated by simultaneously measuring the shift in one of the FBG wavelengths and the change the intensities of R_1 and R_2 as known strains and temperatures were applied. To analyze the reflectance signals, we calculated the function

$$F(R_1, R_2) = \frac{(\sqrt{R_1} - \sqrt{R_2})}{(\sqrt{R_1} + \sqrt{R_2})} \tag{16}$$

which corrects R_1 and R_2 for the double pass through the LPG and normalizes for changes in the overall source intensity. The results for $F(R_1, R_2)$ and λ_{b2} versus strain at a temperature of 38 °C are shown in Fig. 24(a), and similarly the result for $F(R_1, R_2)$ and λ_{b2} versus temperature at an applied strain of 590 μstrain is shown in Fig. 24(b).

Once the sensor was been calibrated, any applied strain and temperature could be simultaneously determined by measuring $F(R_1, R_2)$ and λ_{b2}, then using the known calibrations to solve for the strain and temperature required. The sensor was tested by applying known strains and temperatures, then calculating the values of strain and temperature from $F(R_1, R_2)$ and λ_{b2} and comparing the values. Over the range from 290 μstrain to 1270 μstrain and 25–50 °C, the rms deviation of the measured strain from the applied strain was ± 9 μstrain, and the rms deviation of the measured temperature from the applied temperature was ± 1.5 °C.

A similar measurement can be made using two resonances of a single LPG, provided that the ratio of strain responses in the two resonances is different from the ratio of their temperature responses (i.e., that the determinant of the response matrix is far from zero) [58]. The accuracy of such a system will depend critically on the magnitudes of the responses. We have measured the strain and temperature responses of two resonances in a $L = 210$ μm grating written in AT&T 3D fiber. The resonance wavelengths and responses were 1248 nm, 0.000 97 nm/$\mu\varepsilon$ and 0.074 nm/°C, and 1634 nm, -0.0039 nm/$\mu\varepsilon$ and -0.03 nm/°C. Error propagation analysis for this system shows that if the resonance wavelengths could be determined to ± 0.1 nm, then the strain and temperature could be determined to within ± 31 μstrain and ± 1.5 °C. In an actual system there would also be some uncertainty in the matrix coefficients, which would decrease the accuracy of the strain and temperature measurements, but this ideal case

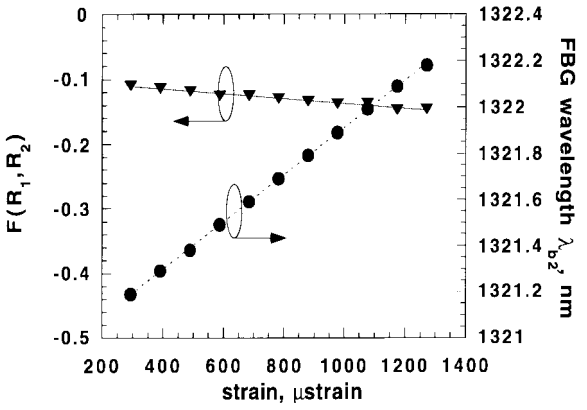

(a)

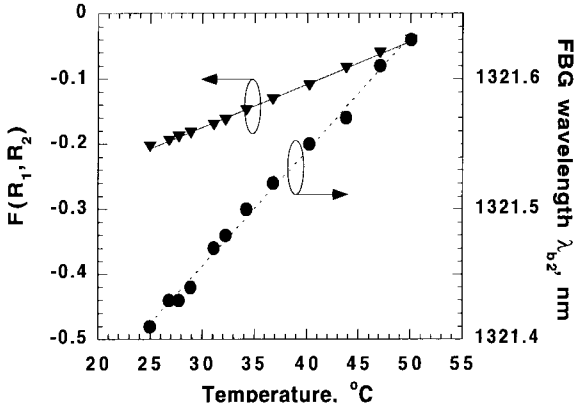

(b)

Fig. 24. (a) $F(R_1, R_2)$ and λ_{b2} versus strain in μstrain, measured while the sensor was held at a temperature of 38 °C, and linear fits to the data. (b) $F(R_1, R_2)$ and λ_{b2} versus temperature in °C, measured while the sensor was held at 590 μstrain applied, and linear fits to the data.

illustrates the potential for multi-parameter sensing using LPG resonances.

An alternative approach for temperature-independent strain sensing is to fabricate LPG's which have no response to temperature, by balancing the temperature responses of the core and cladding effective indices. This ideal has not been realized; however, reduced temperature response has been achieved in fiber with specially tailored refractive index profile (0.0045 nm/°C), [59] with boron-codoped core (0.005 nm/°C) [60], and by using a shorter period ($\Lambda = 40\ \mu$m) grating in a standard fiber (-0.0018 nm/°C) [61].

LPG's have been used in several sensor systems and have some particular advantages. They are the only short-gauge length fiber sensor whose response can be selected for a specific application, and their multiple resonances can be used for simultaneously sensing multiple parameters. Challenges to the widespread use of the devices in structural sensing include developing suitable coatings to protect the fiber, refining interrogation techniques for the resonances, and narrowing the LPG resonance bands to allow multiplexing of the sensors. Finally, the area of environmental monitoring using the sensitivity of the LPG to the surrounding refractive index has not been explored in this review, but it should be an increasingly important application [61].

V. Bragg Grating Laser Sensors

Fiber Bragg gratings are also ideal for use as spectrally narrowband reflectors for creating in-fiber cavities for fiber lasers. This area has attracted interest from both the communications research community for tunable single frequency devices for wavelength division multiplexed networks [63]–[65], and in the sensing field for strain, temperature and very high resolution dynamic strain monitoring. Several variations on this concept have been reported over the past few years.

The basic form of a fiber Bragg grating laser sensor (FBGLS) utilizes either two gratings of matched Bragg wavelength to create an in-fiber cavity, or one grating combined with a broadband reflector. The use of doped fiber section between the gratings or grating and reflector (e.g., erbium) allows the system to be optically pumped to provide cavity gain and thus lasing. The device can be implemented in various ways and operated in either a single frequency or multimode fashion [66]–[68]. When configured as a sensor element, changes in the environmental conditions subjected to the laser cavity and the gratings can be detected by monitoring the change in some characteristic of the output. For strain or temperature variations on the gratings themselves, the shift in wavelength of the laser output is identical to that obtained with the passive approach for monitoring FBG's. With FBG laser sensor configurations, however, it is also possible to detect such effects as the beating between different longitudinal cavity modes or polarization modes in the system [69]. As with basic FBG sensing, the inherent wavelength division addressing capabilities of gratings also allows distributed laser-sensors to be implemented [70], [71].

Fig. 25 illustrates two examples of the types of fiber laser sensors which have been demonstrated. In Fig. 25(a), short cavity fiber lasers created by gratings of matched wavelength are remotely pumped. The grating lasers, which can be as short as $\sim$3 cm in length, behave as sensors with a gage length equal to the length of the cavity, with the same spectral responsivity as a normal FBG element (provide the entire cavity is strained uniformly). The advantage of the laser configuration is, however, the fact that the bandwidth of the output light from the laser sensor can be much narrower than that from a passive FBG sensor system. In Fig. 25(b), a system which incorporates a series of FBG reflectors in a composite cavity configuration is shown [71]. In this system, each laser (defined by the partial broadband reflector and each of the FBG elements) can lase simultaneously. Providing each laser is preset (by the FBG wavelengths) to operate at a nominally different wavelength, the outputs can be analyzed simultaneously using a wavelength detection system of the type described in Section II.

One of the interesting applications of FBG laser sensors is as compact, high sensitivity sensors. The use of a short cavity lasers of the type shown in Fig. 25(a) allows for single frequency operation. The linewidth of the laser output from such lasers has been reported to be less than 50 kHz, which permits the detection of very weak dynamic strain perturbations of the laser cavity. Such cavity perturbations result in low level "frequency-modulation" of the laser out-

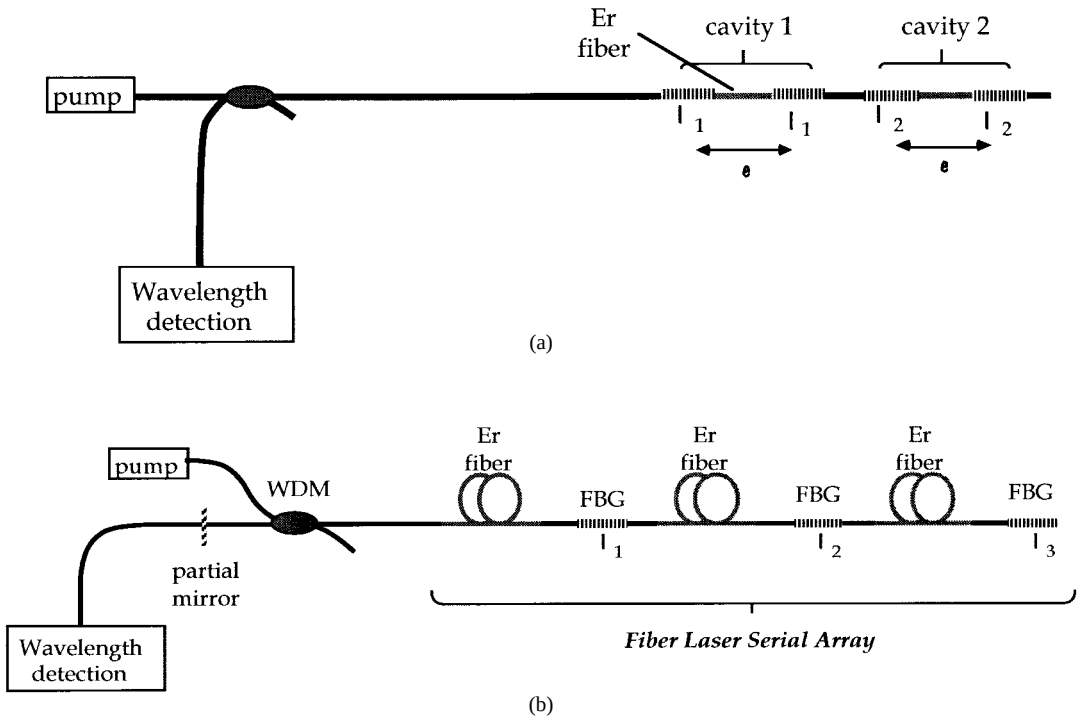

Fig. 25. Basic fiber Bragg grating laser sensor systems: (a) short cavity FBG-pair lasers and (b) extended cavity FBG lasers.

put, and a system capable of resolving very small shifts in the wavelength of the output, such as the unbalanced Mach–Zehnder interferometric technique, can produce a very high sensitivity to weak dynamic strains [72]. Using this approach, strain sensitivities comparable to those normally obtained using direct interferometry are possible, but using a much shorter length of sensing fiber.

The basic principle of this high resolution Bragg grating laser sensor technique is shown in Fig. 26. Light from the grating laser sensor element is directed into an unbalanced Mach–Zehnder interferometer (Section II-C). Wavelength shifts in the FBGLS output are induced by perturbation of the laser cavity. When this interferometric detection approach is used directly with the broadband source light reflected from a single FBG element, the bandwidth of the reflected signal is relatively large (typically, >0.1 nm), and thus the optical path imbalance of the interferometer is restricted to short lengths which are within the effective coherence length of the reflected light. By contrast, in the case of a single frequency FBGLS, the coherence of the laser output is very long (reported measurements indicate many km). This allows a large optical path imbalance to be used, thereby greatly increasing the sensitivity of the system. For example, for an imbalance of 100 m, the wavelength (optical frequency) to phase responsivity is $\approx$3000 rad/GHz. A 1 μrad/$\sqrt{\text{Hz}}$ phase detection sensitivity in the interferometric readout system then produces an ultra high strain resolution of $\sim 2.5 \times 10^{-15}/\sqrt{\text{Hz}}$. This sensitivity could potentially exceed that normally obtained using direct interferometric sensing.

Fig. 27 shows the result of a strain resolution measurement made with a 1555 nm FBGLS ($\sim$3 cm Er cavity) with a 100 m path imbalance readout interferometer. In this case, the FBGLS was surfaced adhered to a piezoelectric strip which could be used to apply strain to the cavity. The single mode output of the FBGLS was coupled to the unbalanced Mach–Zehnder interferometer, and the FBGLS cavity was modulated to induce a phase modulation at the interferometer output. The measurement indicates a phase noise level of $\sim$26 μrad/$\sqrt{\text{Hz}}$ at 7 kHz, which corresponds to strain resolution of the FBGLS cavity of $\sim 5.6 \times 10^{-14}$/AHz, illustrating the ultra high sensitivity of the approach. With this level of strain sensitivity, the fiber Bragg grating laser sensor can be used as a high sensitivity device for sensing, for example, acoustic pressure induced strain, or configured as a compact sensor for the detection of various measurands, such as magnetic fields [73]. The multiplexing of four fiber lasers sensors using a single readout interferometer has been demonstrated [74].

VI. Interferometric Sensors

An additional use of Bragg gratings is to form interferometric sensor elements [75]–[80]. In this case, the gratings serve merely as reflectors which define the interferometric paths. One of the earliest multiplexing techniques demonstrated for interferometric arrays was based on the use of in-fiber partial reflectors, which were formed using mechanical splices between fiber segments of the array [75]. This produced weak reflectivities in the range of a few percent, as required to achieve low crosstalk [76] with the approach. The reflectivities obtained via the mechanical splice were found to be unstable and lossy, thus limiting the usefulness of the technique. The advent of in fiber Bragg gratings, however, provided a practical means of producing reliable, low-insertion loss, in-fiber partial reflectors. Fig. 28 illustrates the configuration [77].

In addition to merely acting as full or partial reflectors, the wavelength selective nature of the gratings provides unique capabilities and configurations to be implemented. The most ob-

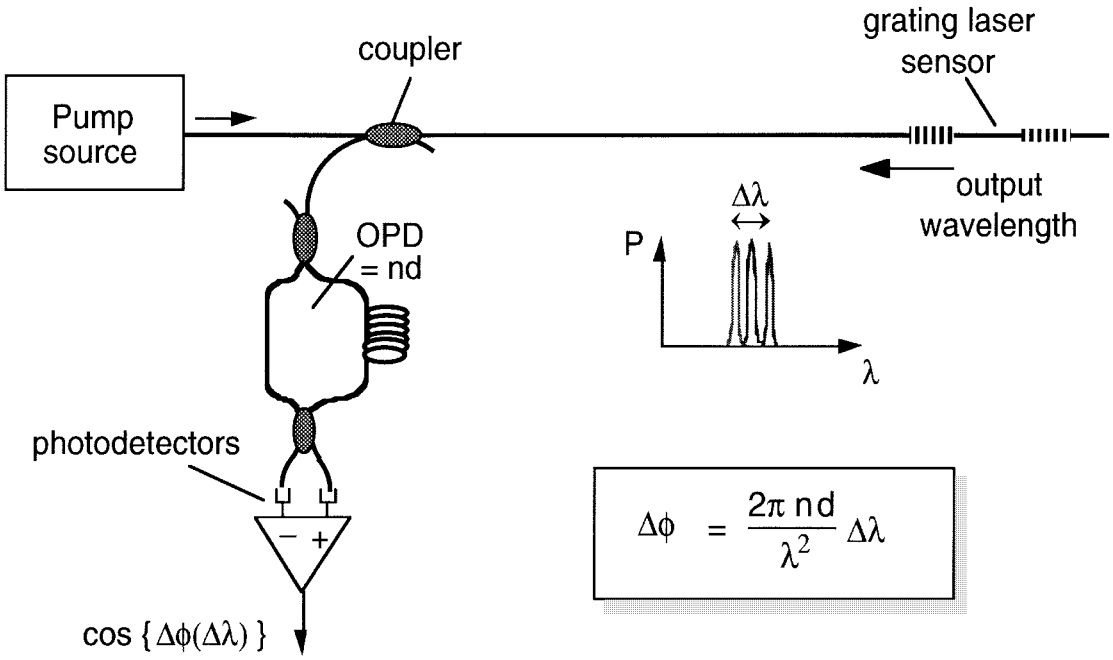

Fig. 26. Basic fiber Bragg grating laser sensor with interferometric detection.

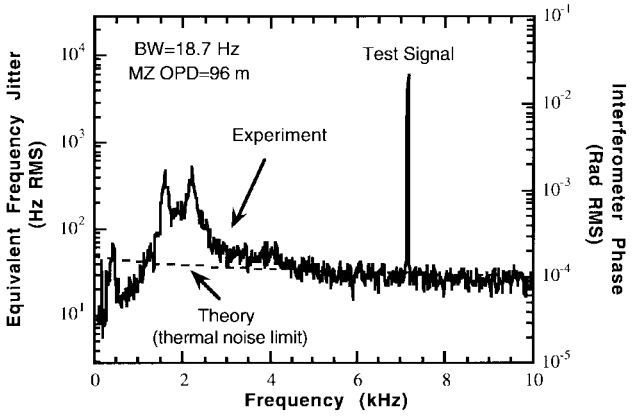

Fig. 27. Sensitivity to weak cavity strain observed using the Bragg grating laser sensor configuration.

vious extension of this is to the implementation of WDM/TDM interferometric arrays [78]. It has also been demonstrated that the use of gratings can allow selective interrogation of overlapping "nested" interferometers implemented in common fiber paths [79]. This sensor concept can be used to form adaptive sensor arrays, or to implement specialized sensor configurations, such as gradient and vector type sensors.

The idea is illustrated in Fig. 29, which shows three examples of the types of configurations which can be implemented using nesting concepts: In Fig. 29(a), an implementation consisting of multiple co-existing interferometers within a single Michelson configuration is shown. The multiple interferometers are formed using a series of Bragg gratings between sensor and respective reference coils, as shown. Due to the wavelength selectivity of the gratings, the system produces an interferometer signal, the phase response of which is determined by the input source wavelength: Interrogation of the system at one of the wavelengths corresponding to one of the grating pairs in the system produces an interferometer output, the phase of which can be described by

$$\phi_{\lambda j} = \sum_{i=1}^{j} \phi_i \tag{17}$$

where ϕ_i is the phase induced in the ith ($i = 1$ to N) sensor coil. The phase response at the jth wavelength is the sum of the phase induced at each sensor coil up to the last addressed element. With this processing, the phase of any given sensor coil (or combination of coils) can be assessed via

$$\phi_j = \phi_{\lambda j} - \phi_{\lambda(j-1)}. \tag{18}$$

As shown, reference coils can be included to maintain the optical path imbalance of each interferometer section constant.

Fig. 29(b) illustrates a Michelson implementation consisting of a $\pm$magnitude/gradient sensor formed by two sensing coils and a single reference length. In this case, with the gratings as shown, interrogation of the system at λ_1 provides a measure of the phase of sensor coil S_1, λ_2 provides a measure of the phase of sensor coil S_2, and λ_3 provides a differential, or gradient, measurement.

In the third example, Fig. 29(c), an implementation of a serial array of sensor coils is shown which can be read independently, in groups, or as an effective single sensor element by choice of the interrogation wavelength. For an interrogation wavelength λ_1, the gratings at λ_1 define a series of sensors comprising single sensing coils which can be interrogated using a pulse source in accordance with the multiplexing technique described in [75]–[77]. At other interrogation wavelengths, the sensors comprise groups of sensing coils, up to the last wavelength (λ_4 in this example), which "sees" only one sensor comprising all the sensing coils. This system represents a basic form of adaptive sensor array. It can operate with different spatial resolution depending on the

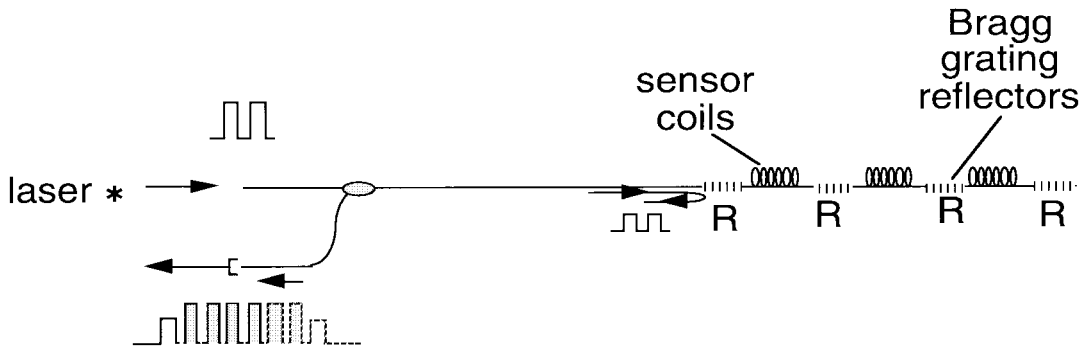

Fig. 28. Serially multiplexed interferometric sensors based on in-fiber grating reflectors.

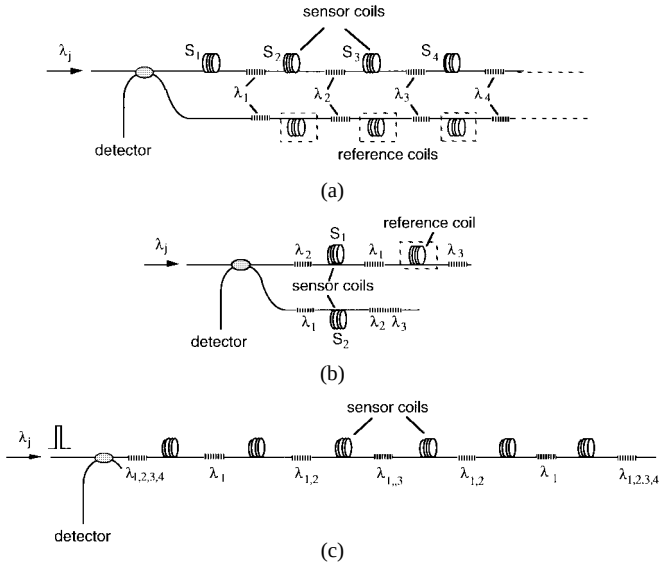

Fig. 29. Nested interferometer configurations. (a) Serial Michelson, (b) implementation for providing ± magnitude and gradient, and (c) nested FP array.

interrogation wavelength. It should be noted that the example shown in Fig. 29(c) represents a very basic geometrically nested array; other more arbitrary nesting implementations, however, could be used.

The nesting of multiple interferometers using common fiber paths provides certain flexibility in designing interferometric sensors, particularly for differential, vector and spatially varying measurands. Nested interferometric arrays based on this concept are possible and may be useful for forming adaptive arrays where the array spatial properties are controlled via the interrogation wavelength.

Other interesting possibilities also exist for implementing novel interferometric sensors such as Michelson's and FP elements using chirped grating reflectors [80].

VII. Summary

There has been very strong research and development interest in fiber grating sensors over the past few years, and this facet of fiber sensor technology currently represents one of the most exciting growth areas in the field. Much of this work is driven by the need to develop distributed strain sensor systems for application in smart structures systems. We have not discussed any of the very significant developments which have occurred in the area of field testing of instrumentation systems, but it should be noted that fiber Bragg grating sensors are being successfully transitioned into real-world applications such as infrastructure [81]–[87] and composite material [88], [89] monitoring, and commercial systems are beginning to emerge. Most of the work done in this area has focused on Bragg gratings, which in addition to their use as direct sensing elements for distributed strain monitoring, can also be used as the fiber sensing element in a host of other applications, such as implementing pressure and acceleration sensors [90], [91]. Some interesting possibilities exist for the development of multiparameter sensor suites based on FBG's. Bragg gratings are also currently being investigated for use in fiber laser sensors configurations, which can be configured for ultrahigh strain sensitivity applications.

Fiber Bragg grating-based sensing has proven to be a very fertile research area, and new developments can be expected to continue over the next few years. In particular, developments utilizing specially modified or tailored gratings, intra-grating concepts, multimode gratings [92], polarization rocking filters [48], long period gratings, π-phase shifted devices [93], and "structured" gratings [94], offer the potential to provide novel and interesting sensing techniques.

Acknowledgment

H. J. Patrick wishes to acknowledge the ASEE for its postdoctoral support.

References

[1] K. O. Hill, Y. Fujii, D. C. Johnson, and B. S. Kawasaki, "Photosensitivity in optical fiber waveguides: Application to reflection filter fabrication," *Appl. Phys. Lett.*, vol. 32, p. 647, 1978.
[2] J. Stone, "Photorefractivity in GeO_2-doped silica fibers," *J. Appl. Phys.*, vol. 62, p. 4371, 1987.
[3] F. P. Payne, "Photorefractive gratings in single-mode optical fibers," *Electron. Lett.*, vol. 25, p. 498, 1989.
[4] D. P. Hand and R. St. J. Russell, "Photoinduced refractive-index changes in germanosilicate fibers," *Opt. Lett.*, vol. 15, p. 102, 1990.
[5] G. Meltz, W. W. Morey, and W. H. Glenn, "Formation of Bragg gratings in optical fibers by a transverse holographic method," *Opt. Lett.*, vol. 14, p. 823, 1989.
[6] R. Kashyap, "Photosensitive optical fibers: Devices and applications," *Optic. Fiber Technol.*, vol. 1, p. 17, 1994.
[7] W. W. Morey, G. Meltz, and W. H. Glenn, "Fiber Bragg grating sensors," in *Proc. SPIE Fiber Optic & Laser Sensors VII*, 1989, vol. 1169, p. 98.

[8] W. W. Morey *et al.,* "Bragg-grating temperature and strain sensors," in *Proc. OFS'89.* Paris, France, 1989, p. 526.

[9] W. W. Morey, J. R. Dunphy, and G. Meltz, "Multiplexing fiber Bragg grating sensors," in *Proc. SPIE Distributed and Multiplexed Fiber Optic Sensors*, Boston, MA, Sept. 1991, vol. 1586, p. 216.

[10] S. M. Melle, K. Liu, and R. M. Measures, "A passive wavelength demodulation system for guided-wave Bragg grating sensors," *IEEE Photon. Technol. Lett.,* vol. 4, p. 516, 1992.

[11] M. A. Davis and A. D. Kersey, "All fiber Bragg grating strain sensor demodulation technique using a wavelength division coupler," *Electron. Lett.,* vol. 30, p. 75, 1994.

[12] Q. Zhang *et al.,* "Use of highly overcoupled couplers to detect shifts in Bragg wavelength," *Electron. Lett.,* vol. 31, p. 480, 1995.

[13] A. B. Lobo Riberio *et al.,* "All-fiber interrogation technique for fiber Bragg grating sensors using a biconical fiber filter," *Electron. Lett.,* vol. 32, p. 382, 1996.

[14] A. D. Kersey *et al.,* "Multiplexed fiber Bragg grating strain sensor system with a fiber Fabry–Perot wavelength filter," *Opt. Lett.,* vol. 18, p. 1370, 1993.

[15] M. A. Davis, D. G. Bellemore, and A. D. Kersey, "Design and performance of a fiber Bragg grating distributed strain sensor system," in *Proc. SPIE 1995 North American Conf. Smart Structures Materials*, San Diego, CA, Feb. 1995, vol. 2446, p. 227.

[16] A. D. Kersey, M. A. Davis, and D. G. Bellemore, "Development of fiber sensors for structural monitoring," in *Proc. SPIE Nondestructive Evaluation of Aging Bridges and Highways*, Oakland, CA, June 1995, vol. 2456, p. 262.

[17] M. A. Davis, D. G. Bellemore, and A. D. Kersey, "Structural strain mapping using a wavelength/time division addressed fiber Bragg grating array," in *Proc. SPIE 1994 2nd European Conf. Smart Struct. Materials*, Glasgow, Scotland, Oct. 1994, vol. 2361, pp. 342–345.

[18] M. G. Xu *et al.,* "Novel interrogation system for fiber Bragg grating sensors using an acousto-optic tunable filter," *Electron. Lett.,* vol. 29, p. 1510, 1993.

[19] J. R. Dunphy *et al.,* "Instrumentation development in support of fiber grating sensor arrays," in *Proc. SPIE Distributed and Multiplexed Fiber Optic Sensors*, Boston, MA, Sept. 1993, vol. 2071, p. 2.

[20] D. A. Jackson *et al.,* "Simple multiplexing scheme for a fiber optic grating sensor network," *Opt. Lett.,* vol. 18, p. 1193, 1993.

[21] M. A. Davis and A. D. Kersey, "Matched-filter interrogation technique for fiber Bragg grating arrays," *Electron. Lett.,* vol. 31, p. 822, 1995.

[22] M. A. Davis, D. G. Bellemore, M. A. Putnam, and A. D. Kersey, "Interrogation of 60 fiber Bragg grating sensors with μstrain resolution capability," *Electron. Lett.,* vol. 32, p. 1393, 1996.

[23] C. G. Askins *et al.,* "Instrumentation for interrogating many-element fiber Bragg grating arrays embedded in fiber/resin composites," in *Proc. SPIE Smart Sensing, Processing and Instrumentation,* 1995, vol. 2444, p. 257.

[24] C. G. Askins, M. A. Putnam, G. M. Williams, and E. J. Friebele, "Stepped-wavelength optical fiber Bragg grating arrays fabricated in line on a draw tower," *Opt. Lett.,* vol. 19, p. 147, 1994.

[25] M. A. Davis and A. D. Kersey, "A fiber Fourier transform spectrometer for decoding fiber Bragg grating sensors," *J. Lightwave Technol.,* vol. 13, p. 1289, 1995.

[26] A. D. Kersey *et al.,* "Polarization-insensitive fiber optic Michelson configuration," *Electron. Lett.,* vol. 26, pp. 518–519, 1991.

[27] M. A. Putnam, M. L. Dennis, J. U. Kang, T. T. Tsai, I. N. Duling III, and E. J. Friebele, "Sensor grating array demodulation using a passively mode locked fiber laser," in *1997 Tech. Dig. Optic. Fiber Commun. Conf.*, J. Onstott, Ed., OSA, vol. 6, p. 156.

[28] T. Morioka, K. Mori, and M. Saruwatari, "More than 100-wavelength-channel picosecond optical pulse generation from a single laser source using supercontinuum in optical fibers," *Electron. Lett.,* vol. 29, p. 862, 1993.

[29] T. A. Berkoff *et al.,* "Hybrid time and wavelength division multiplexed fiber grating array," in *Proc. SPIE,* vol. SPIE-2444. p. 288, 1995.

[30] A. D. Kersey, T. A. Berkoff, and W. W. Morey, "High resolution fiber Bragg grating based strain sensor with interferometric wavelength shift detection," *Electron. Lett.,* vol. 28, p. 236, 1992.

[31] ———, "Fiber optic Bragg grating sensor with drift-compensated high resolution interferometric wavelength shift detection," *Opt. Lett.,* p. 72, 1993.

[32] A. D. Kersey and T. A. Berkoff, "Fiber optic Bragg grating differential temperature sensor," *IEEE Photon. Technol. Lett.,* vol. 4, p. 1183, 1993.

[33] T. A. Berkoff and A. D. Kersey, "Eight element time-division multiplexed fiber grating sensor array with integrated-optic wavelength discriminator," in *Proc. SPIE 1994 2nd European Conf. Smart Struct. Materials*, Glasgow, Scotland, Oct. 1994, vol. 2361, pp. 350–353.

[34] ———, "Fiber Bragg grating array sensor system using a bandpass wavelength division multiplexer and interferometric detection," *IEEE Photon. Technol. Lett.,* vol. 8, p. 1522, Nov. 1996.

[35] M. G. Xu *et al.,* "Discrimination between strain and temperature effects using dual-wavelength fiber grating sensors," *Electron. Lett.,* vol. 30, p. 1085, 1994.

[36] Kanellopoulos *et al.,* "Simultaneous strain and temperature sensing with photogenerated in-fiber gratings," *Opt. Lett.,* vol. 20, p. 333, 1995.

[37] F. Ouellette, "All-fiber filter for efficient dispersion compensation," *Opt. Lett.,* vol. 16, p. 303, 1991.

[38] K. C. Byron, K. Sugden, T. Bricheno, and I. Bennion, "Fabrication of chirped Bragg gratings in photosensitive fiber," *Electron. Lett.,* vol. 29, p. 1659, 1993.

[39] P. C. Hill and B. J. Eggleton, "Strain gradient chirp of fiber Bragg gratings," *Electron. Lett.,* vol. 30, p. 1172, 1994.

[40] M. A. Putnam, G. M. Williams, and E. J. Friebele, "Fabrication of tapered, strain-gradient chirped fiber Bragg gratings," *Electron. Lett.,* vol. 31, p. 309, 1995.

[41] A. D. Kersey, M. A. Davis, and T. Tsai, "Fiber optic Bragg grating strain sensor with direct reflectometric interrogation," in *Proc. 11th Int. Conf. Optical Fiber Sensors, OFS'96*, Sapporo, Japan, May 1996, p. 634.

[42] K. Sugden *et al.,* "Chirped gratings produced in photosensitive optical fibers by fiber deformation during exposure," *Electron. Lett.,* vol. 30, p. 440, 1994.

[43] M. LeBlanc, S. Huang, M. Ohn, R. M. Measures, A. Guemes, and A. Othonos, "Distributed strain measurement based on a fiber Bragg grating and its reflection spectrum analysis," *Opt. Lett.,* vol. 21, pp. 1405–1407, 1996.

[44] M. LeBlanc and A. D. Kersey, "Distributed intra-grating sensing using a chirped fiber Bragg grating and reflection spectrum analysis," *Opt. Lett.,* Mar. 1997, submitted.

[45] S. Huang *et al.,* "A novel Bragg grating distributed-strain sensor based on phase measurements," in *Proc. SPIE Smart Sensing, Processing and Instrumentation,* 1995, vol. SPIE-2444, p. 158.

[46] S. Huang, M. M. Ohn, M. LeBlanc, and R. M. Measures, "Continuous arbitrary strain profile measurements with fiber Bragg gratings," *Smart Materials and Structures,* 1997, to be published.

[47] S. Huang, M. M. Ohn, and R. M. Measures, "Phase-based Bragg intra-grating distributed strain sensor," *Appl. Opt.,* vol. 35, pp. 1135–1142, 1996.

[48] F. Ouellette, "Dispersion cancellation using linearly chirped Bragg grating filters in optical waveguides," *Opt. Lett.,* vol. 12, pp. 847–849, 1987.

[49] M. J. Marrone, A. D. Kersey, and M. A. Davis, "Fiber sensors based on chirped Bragg gratings," in *Proc. OSA Annu. Meeting,* Rochester, NY, Oct. 1996, paper WGG5.

[50] H. Kogelnik, "Filter response of nonuniform almost-periodic structures," *Bell Syst. Tech. J.,* vol. 55, pp. 109–126, 1976.

[51] M. Volanthen, H. Geiger, M. J. Cole, and J. P. Dakin, "Measurement of arbitrary strain profiles within fiber gratings," *Electron. Lett.,* vol. 32, pp. 1028–1029, 1996.

[52] P. Lambelet *et al.,* "Bragg grating characterization by optical low-coherence reflectometry," *Photon. Technol. Lett.,* vol. 5, p. 565, 1993.

[53] A. M. Vengsarkar, P. J. Lemaire, J. B. Judkins, V. Bhatia, T. Erdogan, and J. E. Sipe, "Long-period fiber gratings as band-rejection filters," in *Tech. Dig. Conf. Opt. Fiber Commun.*, San Diego, CA, 1995, postdeadline paper PD4-2.

[54] ———, "Long-period fiber gratings as band-rejection filters," *J. Lightwave Technol.,* vol. 14, pp. 58–64, 1996.

[55] A. M. Vengsarkar, J. R. Pedrazzani, J. B. Judkins, P. J. Lemaire, N. S. Bergano, and C. R. Davidson, "Long-period fiber-grating-based gain equalizers," *Opt. Lett.,* vol. 21, pp. 336–338, 1996.

[56] V. Bhatia and A. M. Vengsarkar, "Optical fiber long-period grating sensors," *Opt. Lett.,* vol. 21, pp. 692–694, 1996.

[57] H. J. Patrick, G. M. Williams, A. D. Kersey, J. R. Pedrazzani, and A. M. Vengsarkar, "Hybrid fiber Bragg grating/long period fiber grating sensor for strain/temperature discrimination," *IEEE Photon. Technol. Lett.,* vol. 8, pp. 1223–1225, 1996.

[58] V. Bhatia, K. A. Murphy, R. O. Claus, and A. M. Vengsarkar, "Simultaneous measurement systems employing long-period grating sensors," in *Conf. Proc. Optic. Fiber Sensors-11 (OFS-11)*, Sapporo, Japan, 1996, pp. 702–704.

[59] J. B. Judkins, J. R. Pedrazzani, D. J. DiGiovanni, and A. M. Vengsarkar, "Temperature-insensitive long-period fiber gratings," in *Tech. Dig. Conf. Opt. Fiber Commun.*, San Jose, CA, 1996, postdeadline paper PD1-1.

[60] K. Shima, K. Himeno, T. Sakai, S. Okude, A. Wada, and R. Yamauchi, "A novel temperature-insensitive long-period fiber grating using a boron-codoped-germanosilicate-core fiber," in *Tech. Dig. Conf. Opt.*

Fiber Commun., Dallas, TX, 1997, pp. 347–348.
[61] V. Bhatia, D. K. Campbell, T. D'Alberto, G. A. Ten Eyck, D. Sherr, K. A. Murphy, and R. O. Claus, "Standard optical fiber long-period gratings with reduced temperature sensitivity for strain and refractive-index sensing," in *Tech. Dig. Conf. Opt. Fiber Commun.,* Dallas, TX, 1997, pp. 346–347.
[62] H. Patrick *et al.,* "Fiber Bragg grating demodulation system using in-fiber long period grating filters," in *Proc. SPIE,* vol. SPIE-2838, p. 60, 1996.
[63] J. L. Zyskind *et al.,* "Short single frequency erbium doped fiber laser," *Electron. Lett.,* vol. 28, p. 1385, 1992.
[64] G. A. Ball *et al.,* "Low noise single frequency linear fiber laser," *Electron. Lett.,* vol. 29, p. 1623, 1993.
[65] G. A. Ball and W. W. Morey, "Compression tuned single frequency Bragg grating fiber laser," *Opt. Lett.,* vol. 19, p. 1979, 1994.
[66] G. Ball *et al.,* "Single and multipoint fiber laser sensors," *IEEE Photon. Technol. Lett.,* vol. 5, p. 267, 1993.
[67] S. M. Melle *et al.,* "A Bragg grating tuned fiber laser strain sensor system," *IEEE Photon. Technol. Lett.,* vol. 5, p. 263, 1993.
[68] A. D. Kersey and W. W. Morey, "Multiplexed Bragg grating fiber laser strain sensor system with mode-locked interrogation," *Electron. Lett.,* vol. 29, p. 112, 1993.
[69] G. Ball *et al.,* "Polarimetric heterodyning Bragg grating fiber laser sensor," *Opt. Lett.,* vol. 18, p. 976, 1993.
[70] A. D. Kersey and W. W. Morey, "Multi-element Bragg grating based fiber laser strain sensor," *Electron. Lett.,* vol. 29, p. 964, 1993.
[71] A. T. Alavie *et al.,* "A multiplexed Bragg grating fiber laser system," *IEEE Photon. Technol. Lett.,* vol. 5, p. 1112, 1993.
[72] K. P. Koo and A. D. Kersey, "Bragg grating based laser sensor systems with interferometric interrogation and wavelength division multiplexing," *J. Lightwave Technol.,* vol. 13, p. 1243, 1995.
[73] K. P. Koo *et al.,* "Bragg grating based laser magnetometer," in *Proc. CLEO'95,* 1995, postdeadline presentation.
[74] K. P. Koo and A. D. Kersey, "Noise and crosstalk of a 4-element serial fiber laser sensor array," in *Tech. Dig. Conf. Opt. Fiber Commun.,* San Jose, CA, vol. 2, p. 226, 1996.
[75] J. P. Dakin *et al.,* "Novel optical fiber hydrophone array using a single laser source and detector," *Electron. Lett.,* vol. 20, pp. 14–15, 1984.
[76] A. D. Kersey *et al.,* "Analysis of intrinsic crosstalk in tapped serial and Fabry–Perot interferometric fiber sensor arrays," in *Proc. SPIE Fiber Optic Laser Sensors VI,* vol. SPIE-985, pp. 113–116, 1988.
[77] W. W. Morey, "Distributed fiber grating sensors," in *Proc. OFS'90,* Sydney, Australia, 1990, p. 285.
[78] S. Vohra, A. Dandridge, B. Danver, and A. Tveten, "An hybrid WDM/TDM reflectometric array," in *Proc. 11th Int. Conf. Optic. Fiber Sensors, OFS'96,* Sapporo, Japan, May 1996, pp. 534–537.
[79] A. D. Kersey and M. J. Marrone, "Nested intererometric sensors utilizing fiber Bragg grating reflectors," in *Proc. 11th Int. Conf. Optic. Fiber Sensors, OFS'96,* Sapporo, Japan, May 1996, pp. 618–621.
[80] A. D. Kersey and M. A. Davis, "Interferometric fiber sensor with a chirped Bragg grating sensing element," in *Proc. OFS-10,* Glasgow, Scotland, 1994, p. 319.
[81] J. D. Proshaka *et al.,* "Fiber optic Bragg grating strain sensor in large scale concrete structures," in *Proc. SPIE Fiber Optic Smart Structures and Skins,* 1992, vol. 1798, p. 286.
[82] R. Maaskant *et al.,* "Fiber optic Bragg grating sensor network installed in a concrete road bridge," in *Proc. SPIE Smart Sensing, Processing and Instrumentation,* 1994, vol. 2191, p. 457.
[83] R. M. Measures *et al.,* "Multiplexed Bragg grating laser sensors for civil engineering," in *Proc. SPIE Distributed and Multiplexed Fiber Optic Sensors III,* 1993, vol. 2071, p. 21.
[84] M. A. Davis *et al.,* "Distributed fiber Bragg grating strain sensing in reinforced concrete structural components," *J. Cement and Concrete Composites,* Aug. 1996.
[85] ———, "High sensor-count Bragg grating instrumentation system for large-scale structural monitoring applications," in *Proc. SPIE North Amer. Smart Structures Meeting,* Feb. 1996, vol. 2718, p. 303.
[86] M. A. Davis *et al.,* "High-strain monitoring in composite-wrapped concrete cylinders using embedded fiber Bragg grating arrays," in *Proc. SPIE North Amer. Smart Structures Meeting,* Feb. 1996, vol. 1721.
[87] S. Huang, M. LeBlanc, M. Lowery, R. Maaskant, and R. M. Measures, "Distributed fiber optic strain sensing for anchorages and other applications," in *Proc. 2nd Int. Conf. Advanced Composite Materials in Bridges and Structures,* 1996, pp. 991–998.
[88] D. Bullock *et al.,* "Embedded Bragg grating fiber optic sensor for composite flexbeams," in *Proc. SPIE Fiber Optic Smart Structures and Skins,* 1992, vol. 1798, p. 253.
[89] E. J. Friebele *et al.,* "Distributed strain sensing with fiber Bragg grating arrays embedded in CRTM composites," *Electron. Lett.,* vol. 30, p. 1783, 1994.
[90] M. G. Xu *et al.,* "Optical in-fiber grating high pressure sensor," *Electron. Lett.,* vol. 29, p. 398, 1993.
[91] T. A. Berkoff and A. D. Kersey, "Multipoint accelerometer system for stuctural monitoring using Bragg grating based transducers," in *Proc. SPIE,* vol. SPIE-2718, paper no. 40, 1996.
[92] K. H. Wanser *et al.,* "Novel fiber devices and sensors based on multimode fiber Bragg gratings," in *Proc. OFS-10,* Glasgow, Scotland, 1994, p. 265.
[93] J. Canning and M. G. Sceats, "π-phase shifted periodic distributed structures in optical fibers by UV post processing," *Electron. Lett.,* vol. 30, p. 1344, 1994.
[94] B. J. Eggleton *et al.,* "Long superstructure Bragg gratings in optical fibers," *Electron. Lett.,* vol. 30, p. 1620, 1994.

Alan D. Kersey received the B.S. degree in physics/electronics from the University of Warwick, U.K., in 1977, and the Ph.D. degree from the University of Leeds, U.K., in 1985.

He joined the Naval Research Laboratory, Washington, DC, in 1984, where he began work on multiplexing techniques for interferometeric sensors. Currently, he is Head of the Fiber Optic Smart Structures Section, which focuses on multiplexed and distributed sensors systems, Bragg grating-based sensors, fiber laser sensors, and general aspects of embedded fiber optic sensors for smart structures.

Michael A. Davis received the B.S. degree in physics from the College of William and Mary, Williamsburg, VA, in 1990, and the Ph.D. degree in physics from the University of Virginia, Blacksburg, in 1997.

Since 1993 he has been working at the Naval Research Laboratory, Washington, DC, in the Optical Sciences Division investigating nonlinear optical processes and optical fiber sensor multiplexing. More recently his research has focused on the use of fiber Bragg grating sensors in smart structures and the development of grating interrogation techniques.

Heather J. Patrick received the B.S. degree in physics from the Massachusetts Institute of Technology (M.I.T.), Cambridge, in 1988, and the Ph.D. degree in physics from the University of Colorado, Boulder, in 1995.

From 1991 to 1995, she was a Graduate Fellow in the Optoelectronics Division of the National Institute of Standards and Technology, Boulder, CO, where she conducted research on the dynamics of Bragg grating growth in germanium-doped optical fiber. Since 1995, she has been an American Society for Engineering Education Postdoctoral Fellow in the Optical Sciences Division of the Naval Research Laboratory in Washington, DC. Her research focuses on the fabrication and modeling of fiber optic devices for use in sensor systems.

Michel LeBlanc received the Bachelor's degree in physics from the Universite de Moncton, Canada, in 1988, and the Master's degree in aerospace science and engineering from the University of Toronto, Toronto, Ont., Canada, in 1990. He is also working towards the Ph.D. degree at the University of Toronto, Institute for Aerospace Studies in the area of fiber optic smart structures.

He is now Research Scientist working for SFA, Inc., Landover, MD, under contract from the Naval Research Laboratory, Washington, DC. His research interests include embedded sensor/ host interaction and Bragg intragrating distributed sensing.

K. P. Koo (S'71–M'77) received the B.S. degree from the University of Illinois-Chicago, in 1972, the M.S. and Ph.D. degrees from the Case Western Reserve University, Cleveland, OH, in 1975 and 1977, respectively, all in electrical engineering.

His research work includes waveguide CO2 laser, optically pumped far infrared laser, laser atmospheric pollutant monitoring systems using intracavity Raman and opto-acoustic schemes, passive and active optical fiber sensors systems, and detection schemes. He has been associated with Brookhaven National Laboratory (1977–1978), John Carroll University (1978–1980) and the Naval Research Laboratory, Washington, DC (on-site contract employee from 1980to present). He holds six U.S. patents and has contributed over 70 journal publications in the area of fiber-optic sensors and laser applications.

Dr. Koo is a member of the OSA.

C. G. Askins, photograph and biography not available at the time of publication.

M. A. Putnam, photograph and biography not available at the time of publication.

E. Joseph Friebele, for a biography, see this issue, p. 1362.